Natural Resources Canada
Ressources naturelles Canada

First results on velocity analyses of multichannel seismic data acquired with the icebreaker RV *Araon* across the southern Beaufort Sea, offshore Yukon

M. Riedel, J.K. Hong, Y.K. Jin, K.M.M. Rohr, and M.M. Côté

Geological Survey of Canada
Current Research 2016-3

2016

Canada

Geological Survey of Canada
Current Research 2016-3

First results on velocity analyses of multichannel seismic data acquired with the icebreaker RV *Araon* across the southern Beaufort Sea, offshore Yukon

M. Riedel, J.K. Hong, Y.K. Jin, K.M.M. Rohr, and M.M. Côté

2016

ISSN 1701-4387
ISBN 978-0-660-05732-3
Catalogue M44-2016/3E-PDF
doi:10.4095/298840

A copy of this publication is also available for reference in depository libraries across Canada through access to the Depository Services Program's Web site at http://dsp-psd.pwgsc.gc.ca

This publication is available for free download through GEOSCAN http://geoscan.nrcan.gc.ca

Recommended citation

Riedel, M., Hong, J.K., Jin, Y.K., Rohr, K.M.M., and Côté, M.M., 2016. First results on velocity analyses of multichannel seismic data acquired with the icebreaker RV *Araon* across the southern Beaufort Sea, offshore Yukon; Geological Survey of Canada, Current Research 2016-3, 24 p. doi:10.4095/298840

Critical review

M.J. Duchesne

Authors

M. Riedel (mriedel@geomar.de)
K.M.M. Rohr (Kristin.Rohr@canada.ca)
M.M. Côté (Michelle.Cote@canada.ca)
Geological Survey of Canada
9860 West Saanich Road
Sidney, British Columbia
V8L 4B2

M. Riedel (mriedel@geomar.de)
Present address: GEOMAR Helmholtz Centre for Ocean Research
Kiel, Wischhofstrasse 1-3, 24148
Kiel, Germany

J.K. Hong (jkhong@kopri.re.kr)
Y.K. Jin (ykjin@kopri.re.kr)
Korea Polar Research Institute
26 Songdomirae-ro, Yeonsu-gu Incheon
406-840 Korea

Correction date:

First results on velocity analyses of multichannel seismic data acquired with the icebreaker RV *Araon* across the southern Beaufort Sea, offshore Yukon

Riedel, M., Hong, J.K., Jin, Y.K., Rohr, K.M.M., and Côté, M.M., 2016. First results on velocity analyses of multichannel seismic data acquired with the icebreaker RV *Araon* across the southern Beaufort Sea, offshore Yukon; Geological Survey of Canada, Current Research 2016-3, 24 p. doi:10.4095/298840

Abstract: One thousand two hundred twenty kilometres of multichannel seismic data were acquired in the Beaufort Sea in 2013 and 2014 to interpret shallow sedimentary structures associated with the upper Cenozoic Iperk and Shallow Bay depositional sequences. Seismic velocity analyses suggest a remarkably consistent regional velocity-depth trend on the slope within the upper 4 s two-way traveltime. A separate velocity trend was not defined beneath the shelf in this region, where data are influenced by the occurrence of permafrost. Deviations from this trend were noted at unconformities including an upper erosional unconformity.

The seismic data in the Mackenzie Trough region suggest a different velocity-depth trend within the upper section and the region is marked by a large erosional unconformity, likely the base of the Shallow Bay sequence. Velocity analyses suggest the removal of up to 425 m of overburden; however, this is an overestimate of erosion as differential compaction from the glacial history has not yet been taken into account. In deeper water (>750 m) a bottom-simulating reflector is present, characterized by the occurrence of free gas and a low-velocity zone.

Analyses of three fluid-expulsion features on the slope indicate that the Pokak fluid-expulsion feature and the Triple-Mound fluid-expulsion feature are linked to underlying anticline structures. A flat-topped fluid-expulsion feature at the flank of an equivalent anticline was also examined, but the occurrence of shallow gas creates a blank zone beneath this structure. Pronounced changes in the velocity-depth function at these fluid-expulsion features are linked to occurrence of free gas, and/or fluidized mud extrusions.

Résumé : En 2013 et 2014, des données sismiques multicanal ont été acquises sur 1220 km dans la mer de Beaufort afin d'interpréter les structures sédimentaires à faible profondeur associées aux séquences sédimentaires d'Iperk et de Shallow Bay du Cénozoïque supérieur. Des analyses de la vitesse sismique indiquent une tendance vitesse-profondeur remarquablement constante à l'échelle régionale sous le talus pour les quatre premières secondes de temps de trajet double. Dans cette région, nous n'avons pas défini une tendance vitesse-profondeur distincte pour le secteur sous-jacent à la plate-forme continentale, un endroit où les données sont influencées par la présence de pergélisol. Des écarts par rapport à la tendance ont été relevés au niveau de discordances, notamment d'une discordance d'érosion supérieure.

Dans la région de la cuvette de Mackenzie, les données sismiques révèlent une tendance vitesse-profondeur différente dans la partie supérieure de la coupe et la région est marquée par la présence d'une importante discordance d'érosion, qui correspond vraisemblablement à la base de la séquence de Shallow Bay. Les analyses de la vitesse laissent croire à la suppression de terrains de couverture sur une épaisseur pouvant atteindre 425 m. Cependant, il s'agit là d'une surestimation de l'importance de l'érosion, étant donné que la compaction différentielle liée à l'histoire glaciaire n'a pas encore été prise en compte. Dans les eaux plus profondes (>750 m), on observe un réflecteur de simulation du fond marin, caractérisé par la présence de gaz libre et d'une zone lente.

Des analyses de trois entités d'expulsion de fluides dans le talus indiquent que l'entité Pokak et l'entité Triple-Mound sont liées à des structures anticlinales sous-jacentes. Une autre entité d'expulsion de fluides à sommet plat, sur le flanc d'un anticlinal équivalent, a également fait l'objet d'un examen, mais la présence de gaz à faible profondeur crée une zone aveugle sous cette structure. Des changements marqués de la fonction vitesse-profondeur au niveau de ces entités d'expulsion de fluides sont liés à la présence de gaz libre ou à des extrusions de boues fluidisées.

INTRODUCTION

Arctic continental shelf regions with water depths of less than 100 m comprise 30% of the total area of the Arctic Ocean. Throughout the Quaternary, the Arctic shelf experienced a varied climatic and thus dynamic geological history. During periods of low sea level, many of these marine shelf areas were not covered with water, but were exposed to mean annual air temperatures of –20°C or colder (Brigham and Miller, 1983). These cold temperatures allowed the development of permafrost and established favourable pressure and temperature conditions for gas-hydrate formation. In contrast, sea-level rise during interglacial periods resulted in marine transgression, yielding the degradation of offshore permafrost and gas-hydrate deposits. The repeated changes between permafrost formation during terrestrial exposure and warming and associated degradation during marine transgression have had substantial impacts on the geology of Arctic continental shelves and slope regions, in the form of e.g. fast-changing styles of sedimentation pattern and sediment types, erosion and redeposition, mass-transport deposits, changes to the fluid-flow pattern, and changes in sediment compaction.

The Arctic continental shelf and slope regions contain substantial offshore hydrocarbon resources, and new phases of exploration and development are expected. The geological processes mentioned above can result in the occurrence of significant geohazards (Hovland et al., 2011), therefore there is the need to identify and quantify these geohazards, and ultimately define the risks of drilling and production activities.

To increase knowledge of geohazards in the Beaufort region, two research expeditions with the Korean icebreaker RV *Araon*, operated by the Korea Polar Research Institute (KOPRI), were undertaken, with an emphasis on collecting targeted 2-D multichannel seismic data (Jin et al., 2015; Jin and Dallimore, 2016). During expedition ARA04C (2013) and ARA05C (2014) a total of 1220 line kilometres of multichannel seismic data were acquired (Fig. 1). Initial

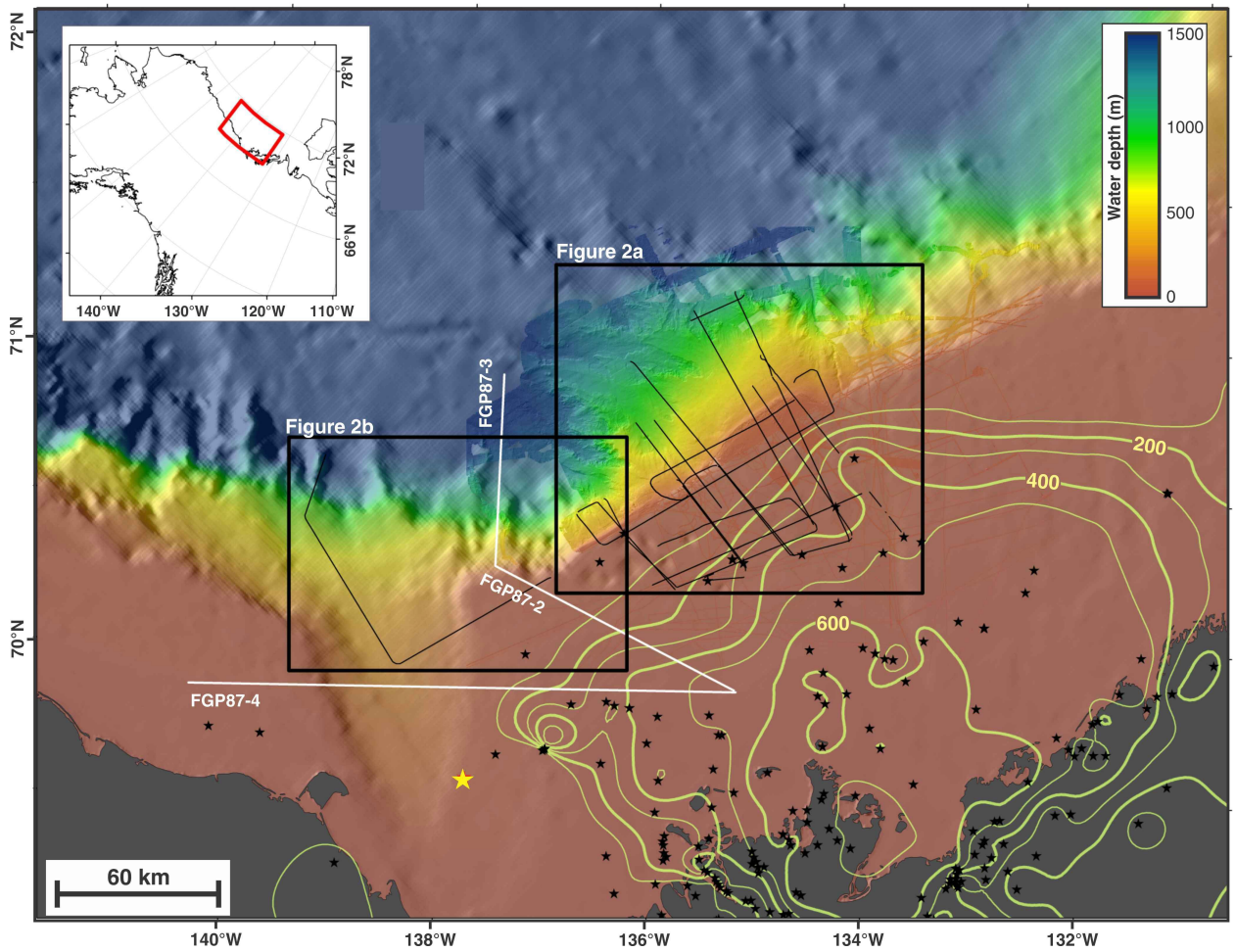

Figure 1. Overview map of study region in the southern Beaufort Sea. Locations of the RV *Araon* multi-channel seismic data are shown as black lines. Thickness of the relict permafrost is shown as yellow contour lines. Industry wells (from which depth of permafrost was defined) are shown as black stars. The Adlartok P-09 well is highlighted as a yellow star. For details *see* text.

processing of these lines focused on the determination of sediment velocities from refractions to define permafrost distribution (Riedel et al., 2014), following work conducted by the Geological Survey of Canada in the mid-1980s (e.g. Pullan et al., 1987). In this study the authors present initial multichannel seismic data results to a record length of 10 s (two-way traveltime) to image the seismic structure of the slope and shelf-edge region and to determine the regional velocity field to aid in geohazard assessments. A second objective of this study is to image the deeper structure of fluid-expulsion features that occur on the slope, previously imaged with high-resolution 3.5 kHz subbottom profiler data (e.g. Blasco et al., 2013; Paull et al., 2015). The multichannel seismic data allow a time-to-depth conversion and definition of the source region of the fluid-expulsion features. Industry 3-D seismic data available on the slope over three prominent fluid-expulsion features are truncated at 2.25 s (two-way traveltime) and thus do not allow imaging of the source region. The study region is split into two subregions: a central region (Fig. 2a) around the main ArcticNet bathymetry data set with acquisition of 12 lines in 2013 and 17 lines in 2014, and a western region (Fig. 2b) in the area of the Mackenzie Trough with the acquisition of three lines in 2014.

SEISMIC DATA ACQUISITION AND PROCESSING

The multichannel seismic system onboard the RV *Araon* comprises an eight airgun array, with maximum volume of 1200 in^3 (19.7 L) and a 120-channel streamer with a 1500 m long active section (Jin et al., 2015). Offsets vary depending on the layout and pay-out distance of the cable, with the maximum offset during the 2014 survey of 1654 m. A standard geometry of the airgun system is shown in Figure 3.

During the 2013 survey, airgun operations were often interrupted due to the occurrence of sea ice, high winds, and air-pressure fluctuations. Data acquisition in 2014 was more stable and data from that survey are more laterally coherent.

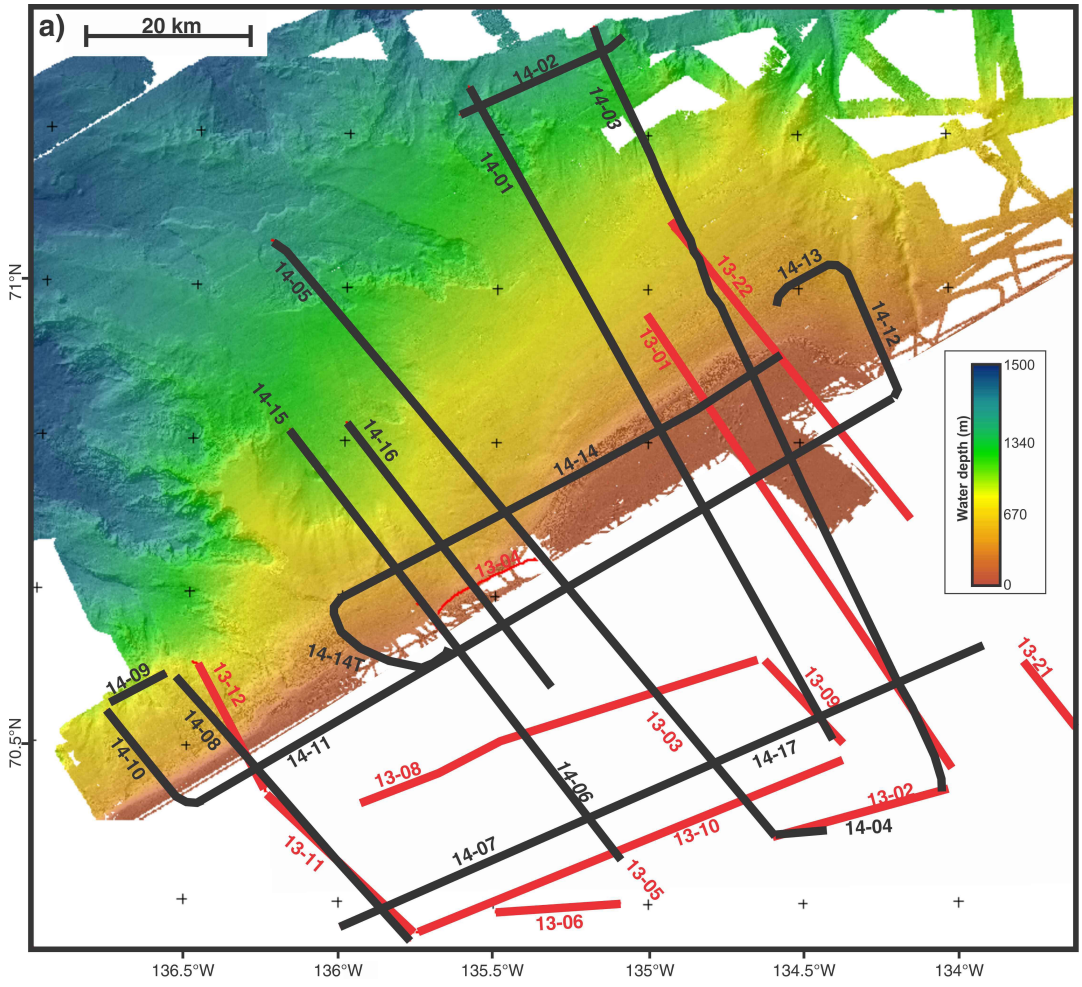

Figure 2. Map of the study regions showing bathymetry from the ArcticNet data set (Blasco et al., 2013) and 2-D seismic coverage from the RV *Araon* expeditions ARA04C (red lines) and ARA05C (black lines); **a)** central study region;

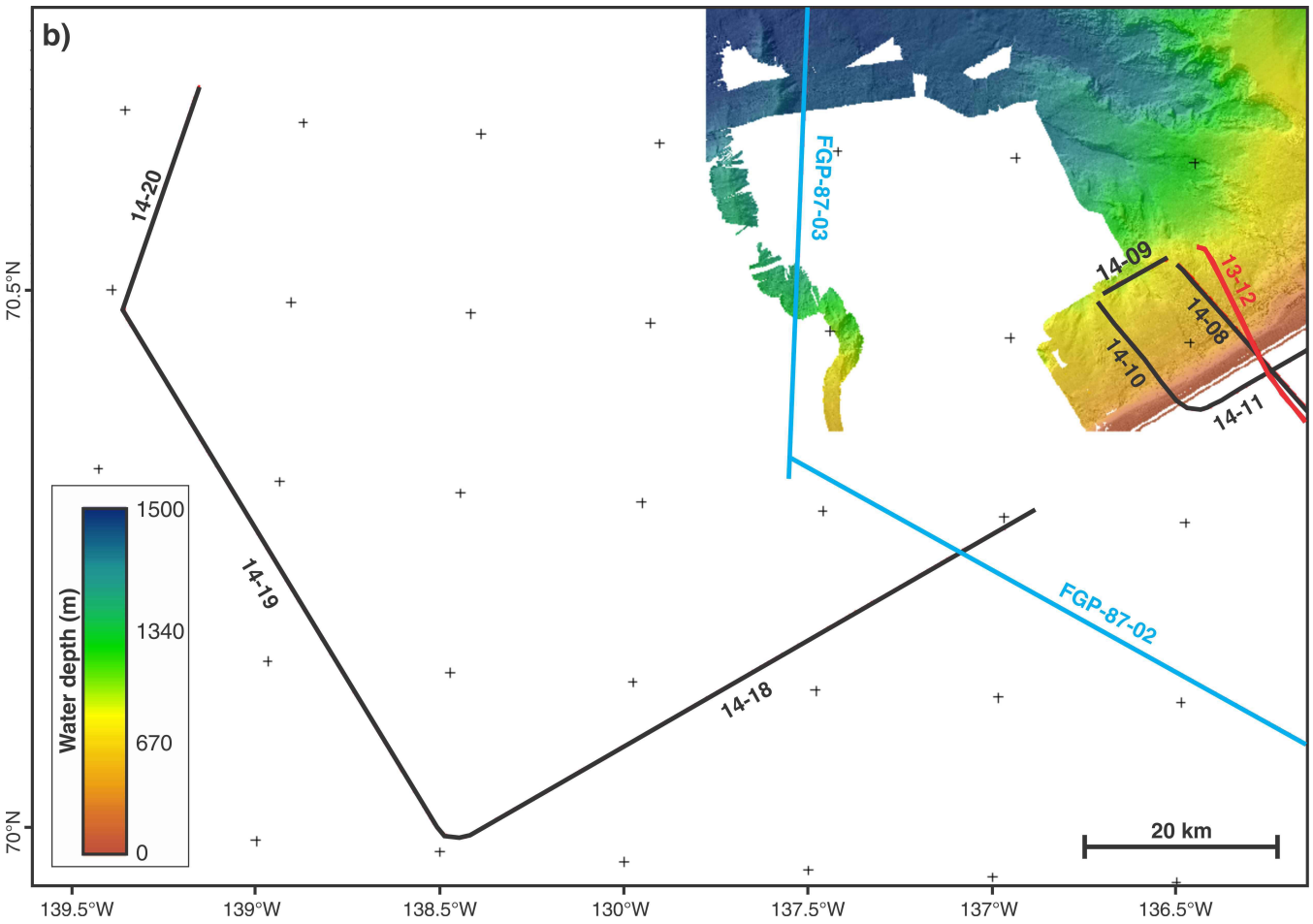

Figure 2. (cont.) b) western study region including the Mackenzie Trough (lines 14-18–14-20) and two lines from the Frontier Geoscience Program (FGP) in blue (Dietrich et al., 1989).

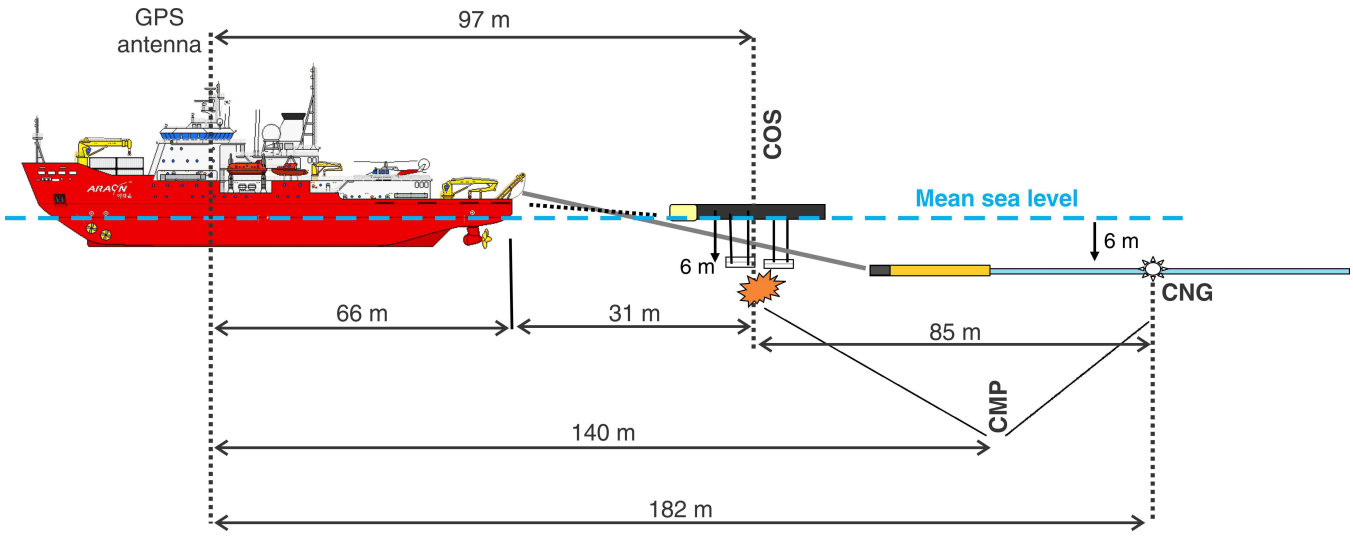

Figure 3. Image showing the basic geometry of the seismic and navigation systems onboard the RV *Araon* (*after* Jin et al., 2015); COS = centre of shot, CNG = centre of near-group, CMP = common midpoint.

The final multichannel seismic processing sequence applied to the data are listed in Table 1. The authors used the processing package Globe Claritas for this task. A trigger-time delay of about 60 ms was identified after initial processing of several lines, and comparison was made to seafloor depths defined from other sources. Subsequently, a vertical bulk shift was applied in the shot-gather domain. A surgical mute was applied to remove refracted arrivals, particularly on the shallow shelf portion of the data set.

The processing used in this study is mainly aimed at preserving the true-amplitude nature of the data. During the analysis, the authors tested several additional processing methods to improve imaging; however, none were found to be satisfactory:

- FK-filtering to remove linear noise (surgical muting was more efficient and did not create artificial noise as the FK-filter did);
- τ-p forward and inverse filtering to remove linear noise and increase fold of the common-depth-point gathers (does not preserve true amplitude); and
- Prediction-error filtering to remove short-period multiples (does not work well on lines with varying water depths).

Table 1. Seismic processing sequence applied.

Processing flow	Processing	Comment
1	Geometry: define field record number (consecutive) and offset of channels, common-depth-point calculation	Crooked line, streamer assumed straight; deviations in line directions result in too short offsets; no feathering correction applied; common-depth-point binning to reduce number of dropped traces
2	Surgical mute of first arrivals and refractions	Shot-gather domain
3	Debias of 0 Hz component	Removal of direct-current component
4	Band-pass filter	Frequency trapezoid: 5–10–200–240 Hz (minimum phase as prerequisite for deconvolution)
4	Surface-consistent deconvolution	200 ms operator length, 16 ms gap length
5	Common-depth-point sorting	Crooked-line approach
6	Constant-velocity stack	Brute-stack for detailed velocity analysis application
7	Semblance-based velocity definition	Root-mean-square velocity
8	2-D varying spherical divergence correction	On common-depth-point gathers
9	Normal move out and stack	Stack normalized by number of traces in common-depth-point gather
10	Hyperbolic radon transform to remove long-period multiples	Iterative process; 2nd application of velocity analysis (step 8) after first demultiple process
11	Time migration finite difference Kirchhoff	Two migrations for comparison purposes
12 (optional)	Spectral whitening	Frequency trapezoid: 5–10–150–200 Hz
13 (optional)	Automatic gain control	1 s window length for image enhancement
14 (optional)	Zero-phase filter	On migrated section
15 (optional)	Deconvolution	Poststack signature deconvolution
16 (display purpose)	Depth-conversion from root-mean-square to interval	Dix (1955) equation

The authors found that for the portion of the data across the slope in water depths exceeding 140 m, multiple-removal processing with such as the hyperbolic radon transform (e.g. Foster and Mosher, 1992) was not necessarily required if the velocity definition clearly excluded the water-bottom multiple. Stacking of the traces within a common depth point alone reduced multiple energy and preserved primary reflections sufficient for some initial interpretation. On the shelf, however, data are degraded from the shallow-water multiples and refractions down to a depth of about 1 s two-way traveltime. Imaging beneath the shelf below this depth is possible, though absorption of seismic energy from the hard bottom and from the permafrost reduced the total imaging depth and quality of the data (as well as a reduction of frequency content). A more detailed evaluation of de-multiple processing algorithms is required, but is beyond the scope of the initial processing evaluation.

As deeper structures (i.e. below ~4 s two-way traveltime) of the underlying fold-and-thrust belt (*see* details in Pelletier, 1988) were imaged by the RV *Araon* multichannel seismic data, significant dip was identified. A dip moveout processing sequence may be required to improve definition of the velocity trend and help increase the signal-to-noise ratio on the stacked images. Prestack migration may also help address this issue.

STRATIGRAPHIC AND STRUCTURAL SETTING

The uppermost sedimentary sequences (upper 2–4 km) within the Beaufort-Mackenzie Basin are comprised of two main depositional sequences (e.g. Dixon and Dietrich, 1990; Dixon et al., 1992; Dixon, 1996): the Iperk sequence (early Pliocene to mid-Pleistocene) and the Shallow Bay sequence (mid-Pleistocene to Holocene, although no dates have been obtained from samples). The regional unconformity associated with the base of the Iperk sequence was previously defined (e.g. Dietrich et al., 2010) as a regional unconformity separating layers with pervasive tectonic deformation from undeformed layers and is at a depth of about 2.5 s two-way traveltime (equivalent to a depth of 2.8–3.5 km (Dietrich et al., 2010)) below seafloor across the shelf. The newly acquired 2-D multichannel seismic data (shown in Fig. 4a–4f) can be used to define this sequence boundary across the slope region and can tie the depth definition back to the lower resolution, vintage, redigitized industry seismic records.

In an interpretation by Dietrich et al. (2010) of one seismic line across the outer Mackenzie Trough, the top of the Iperk sequence (base of Shallow Bay) is marked by a transition from the underlying higher amplitude, more deformed sequence to the mostly lower amplitude, sedimentary reflections above. The base to the Shallow Bay sequence was initially defined on the shelf of the Mackenzie Trough by Dietrich et al. (1989) as a prominent angular unconformity seen in vintage seismic-reflection data. On the nearby slope, an unconformity separating nearly transparent from reflective layers in seismic line FGP-87-03 (Frontier Geoscience Program) (Dietrich et al., 1989) was interpreted to be the same unconformity (Dietrich et al., 2010), but was not directly tied to the lines where it was initially defined. Since then, interpretations of recent data in the Mackenzie Trough indicate that this sequence was primarily deposited by an ice stream (Batchelor et al., 2013a) and is no older than Illinoian.

Multiple erosional processes shaped the sediment packages of the upper slope (K.M.M. Rohr, M. Riedel, and S.R. Dallimore, unpub. manuscript, 2016), and therefore it has proved difficult to define a single unconformity as the base of the Shallow Bay sequence. Line spacing is sparse in the deep-water portion of the survey area and despite two available 3-D seismic volumes, regional mapping of these unconformities is challenging and beyond the scope of this study. Where possible, the approximate depths of these sequence boundaries were defined using amplitude variations and erosional character as possible indicators. In the remaining section, the authors focus on the velocity definition and changes around the possible depth of these unconformities, as well as fluid-expulsion features.

The seismic data from the Mackenzie Trough region show the dominant erosional base of glacial scouring from ice advance (Fig. 4g, 4h). This marked unconformity is underlain by tilted and faulted sediment packages. Above the glacial erosional surface, sediments are a mix of glacial till and sand sequences (e.g. Batchelor et al., 2013a) showing small-scale semiparallel reflection packages. An upper veneer of laminated postglacial sediments can be identified. The base of the glacial scour within the Mackenzie Trough is likely correlated with the base of the Shallow Bay sequence. The depth to this unconformity mapped by Batchelor et al. (2013a) matches the depth defined in the Adlartok P-09 well (Fig. 1) (Dixon et al., 1992).

SEISMIC VELOCITY DEPTH TRENDS

Deep-water baseline trend

Using the basic seismic processing sequence outlined in Table 1, the authors carried out a seismic stacking velocity definition using the semblance technique. Stacking velocities maximize the stack power within a common depth point, yielding the optimal stacked image and are approximately equal to root-mean-square values allowing an interpretation for interval velocities (Dix, 1955). The present authors first defined a regional deep-water (>780 m) background trend for comparison purposes (Fig. 5a). During the semblance analyses, the authors noted a remarkably similar and almost linear root-mean-square velocity depth trend from all lines.

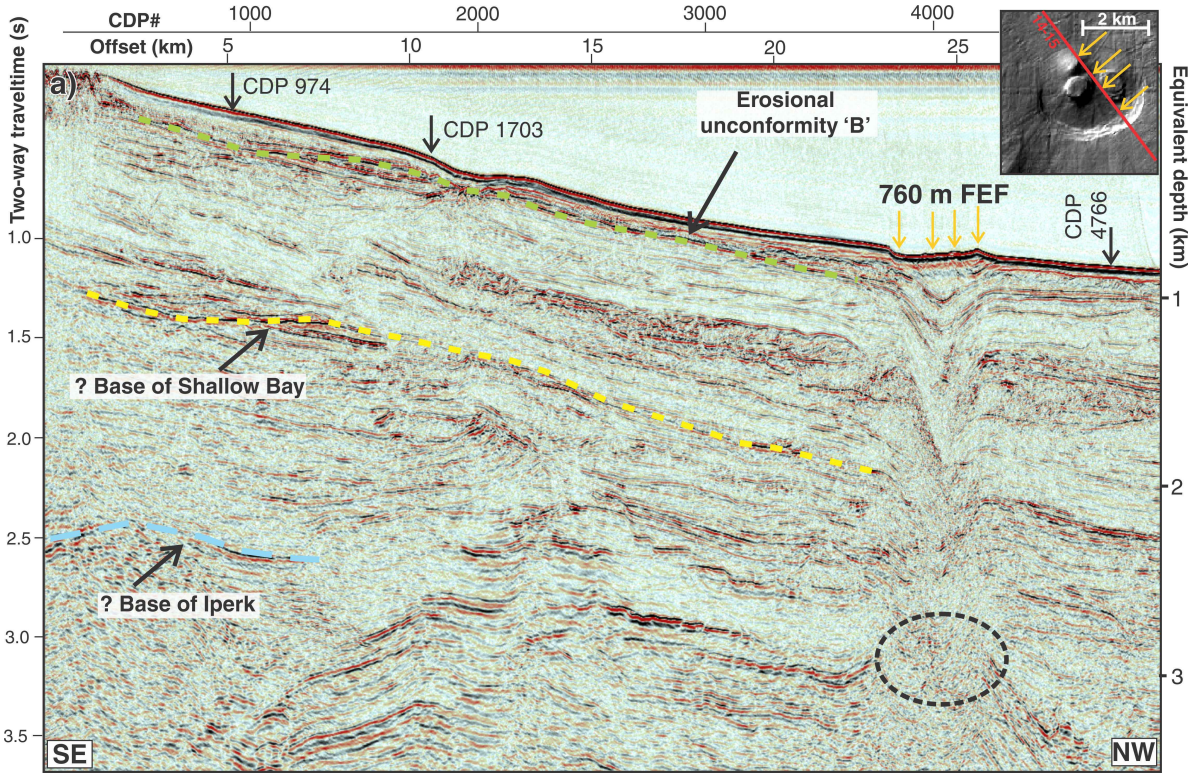

Figure 4. Images of multichannel seismic Kirchhoff time-migrated data from ARA05C. An approximate depth scale is shown on the right of each image. An automatic gain control (AGC) with a 1.0 s operator length is used for display purposes. The approximate location of unconformities associated with the base of the Shallow Bay and Iperk sequences are identified where possible. The base of the Iperk sequence (blue) was identified as a cessation of tectonic activity; a possible location of the base of the Shallow Bay sequence (yellow) was identified as occurring at a similar time to its interpreted time near the Mackenzie Trough (Dietrich et al., 2010). **a)** Section of line 14-15; the source region of the 760 m fluid-expulsion feature (FEF) is shown by the dashed circle. Locations of common depth points (CDPs) used for semblance analyses shown in Figures 6d and 6e are indicated by small black arrows. Upper inset shows shaded-relief multibeam map of the 760 m fluid-expulsion feature and location of line 14-15 with the four common depth points shown in Figure 6e identified by yellow arrows.

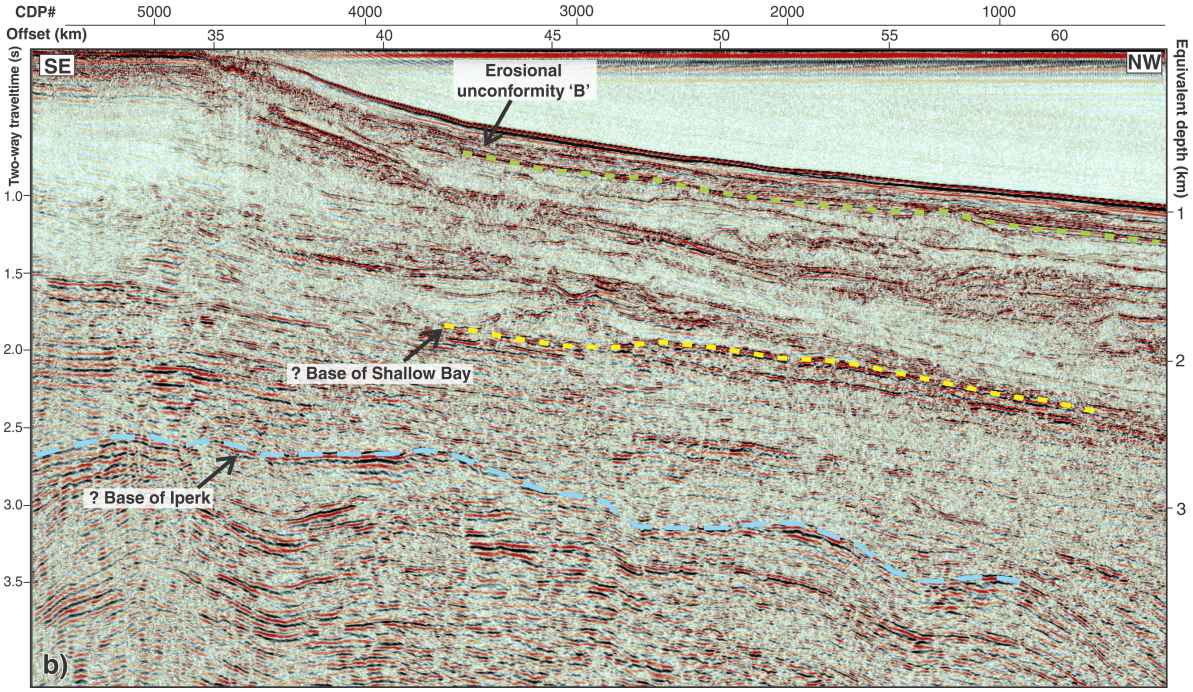

Figure 4. (cont.) **b)** Section of line 14-16; three unconformities are identified. CDP = common depth point

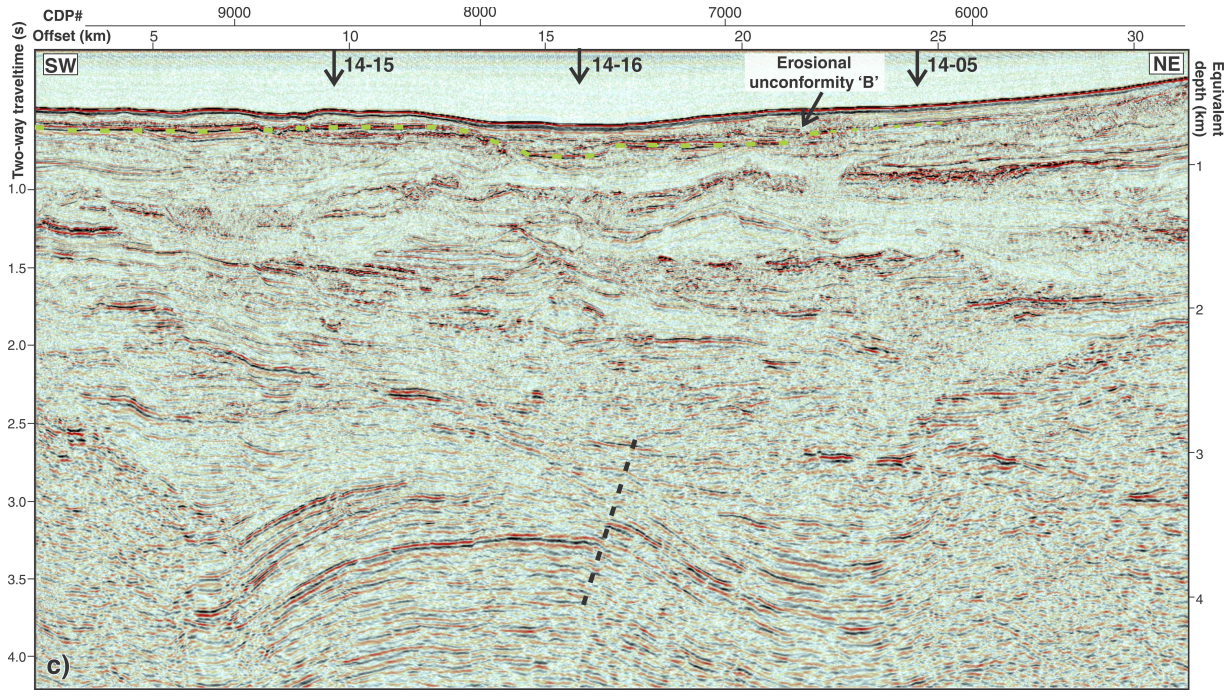

Figure 4. (cont.) c) Section of line 14-14; the uppermost unconformity is identified, whereas the base of Iperk and Shallow Bay sequences are difficult to assign, although the folded sediments below the Iperk sequence can be clearly seen. Black dashed line indicates a fault. CDP = common depth point

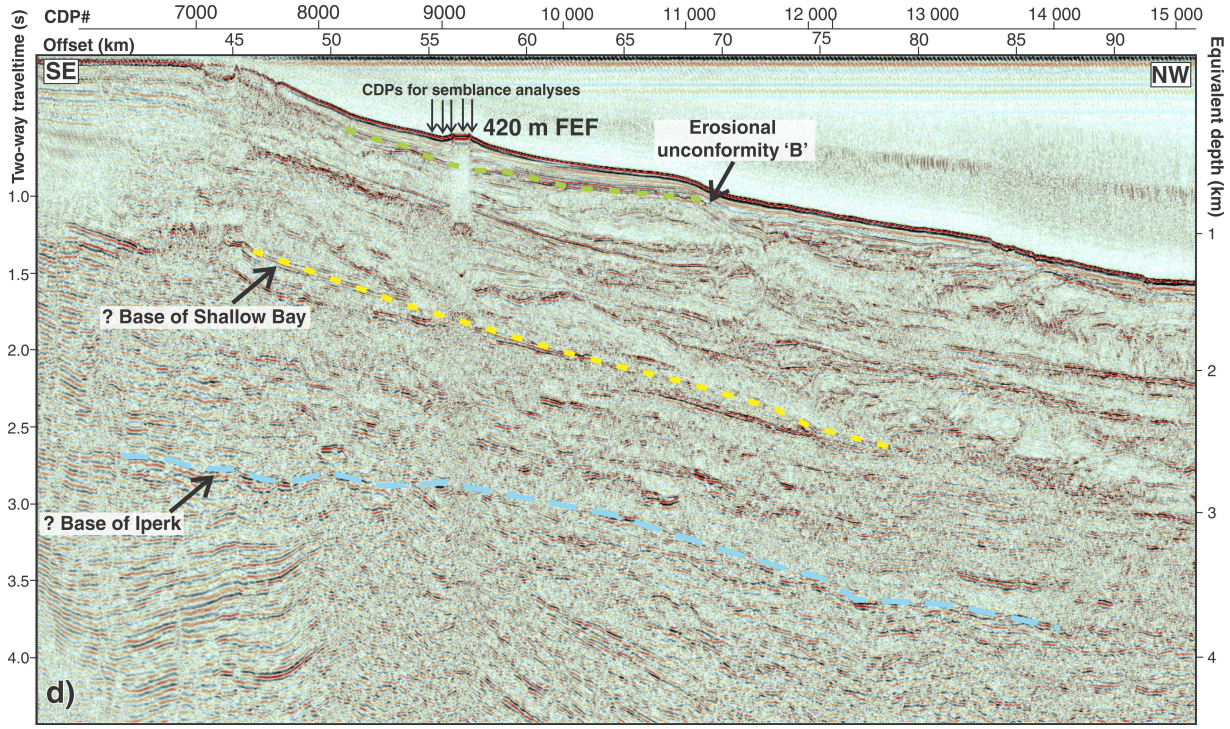

Figure 4. (cont.) d) Section of line 14-05; three unconformities are identified. Note the folded sequence of sediments beneath the inferred base of Iperk sequence. CDP = common depth point, FEF = fluid-expulsion feature

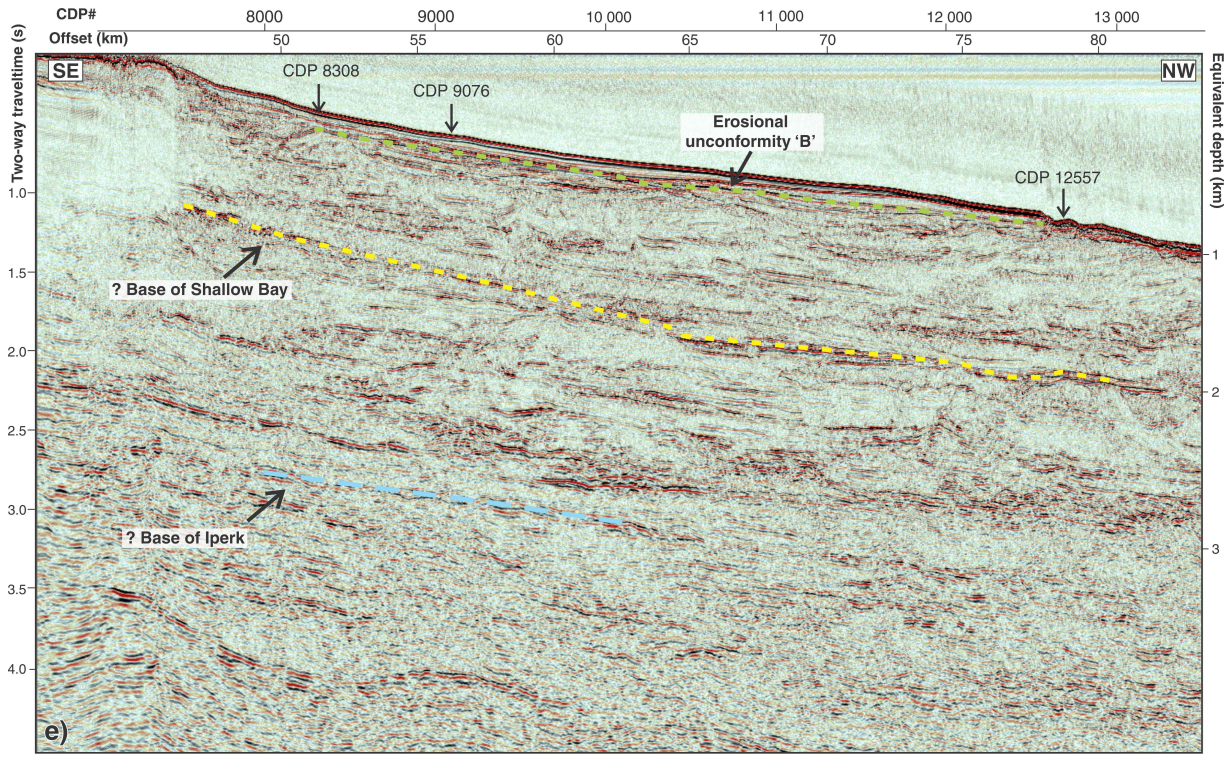

Figure 4. (cont.) e) Section of line 14-01; three unconformities are identified. Locations of common depth points (CDPs) shown in semblance analysis (*see* Fig. 6a) are indicated by black arrows. Note the folded sequence of sediments beneath the inferred base of Iperk sequence.

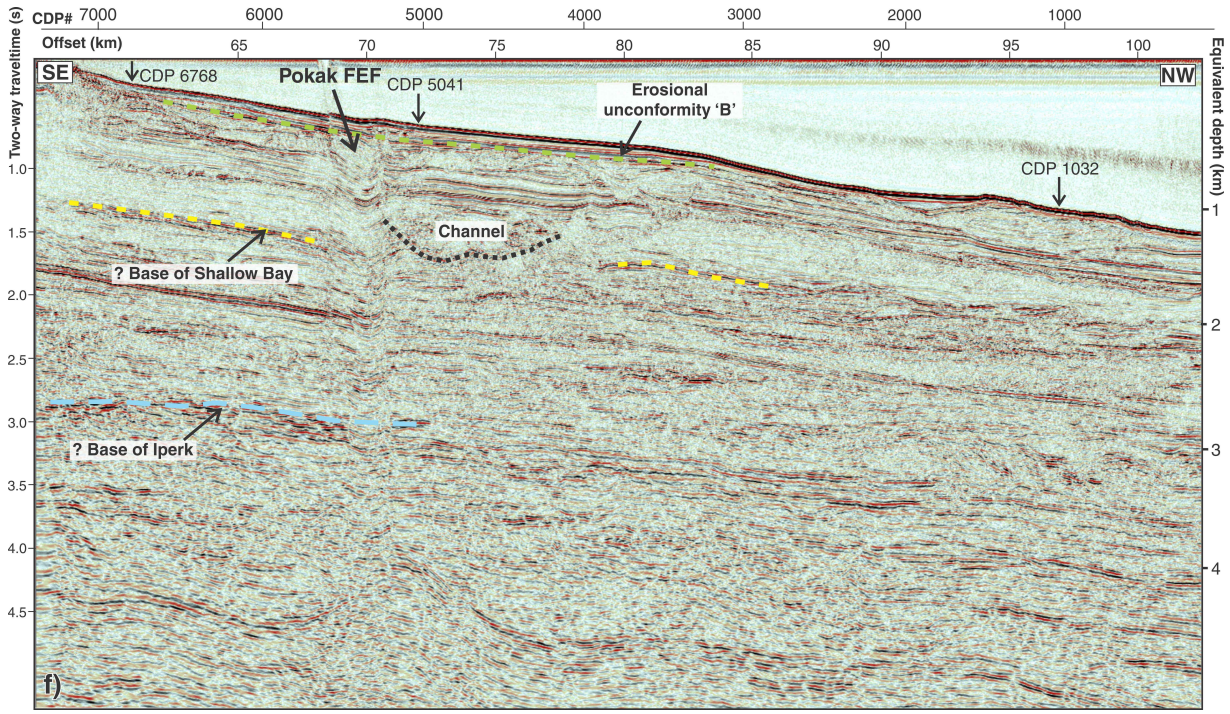

Figure 4. (cont.) f) Section of line 14-03; three unconformities are identified. Locations of common depth points (CDPs) shown in Figure 6b are indicated by black arrows. Note the folded sequence of sediments beneath the inferred base of Iperk sequence, especially the link between a fold and the location of the Pokak fluid-expulsion feature (FEF).

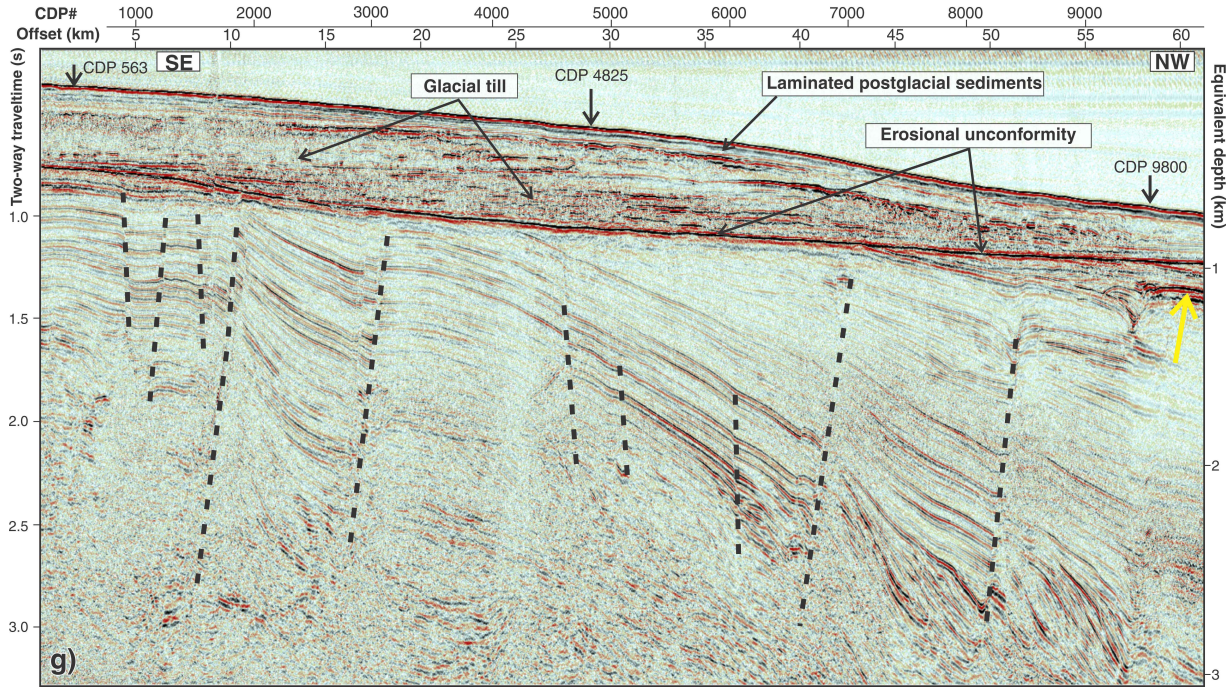

Figure 4. (cont.) g) Section of line 14-19; note the strongly faulted nature of sediments beneath the erosional unconformity. Locations of common depth points shown (CDPs) in Figure 6 are indicated by black arrows. The bottom-simulating reflector is indicated by a yellow arrow.

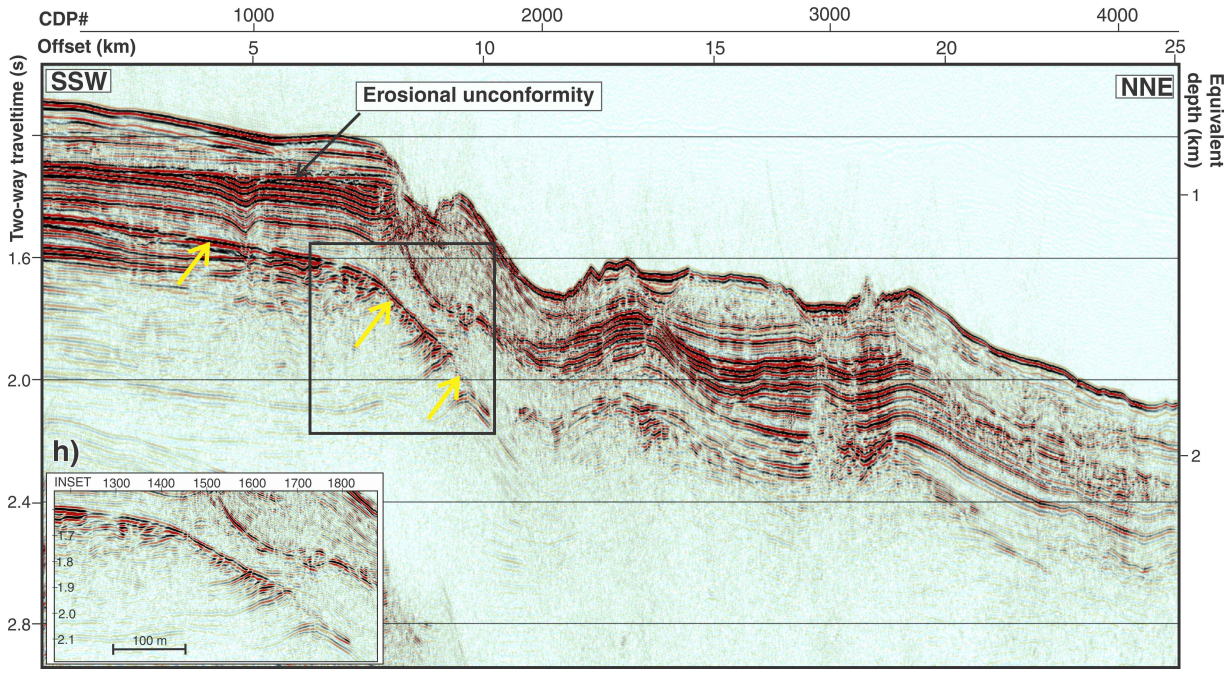

Figure 4. (cont.) h) Section of line 14-20; no automatic gain control was used to highlight the presence of the potential bottom-simulating reflectors between common depth points (CDPs) 100–1820. The bottom-simulating reflector is indicated by yellow arrows. The inset at the lower left corner shows a detailed image around the bottom-simulating reflector–like event. The reflection identified could be another erosion unconformity, as sedimentary layers are apparently cut off at the bottom-simulating reflector–like event and are not through-going.

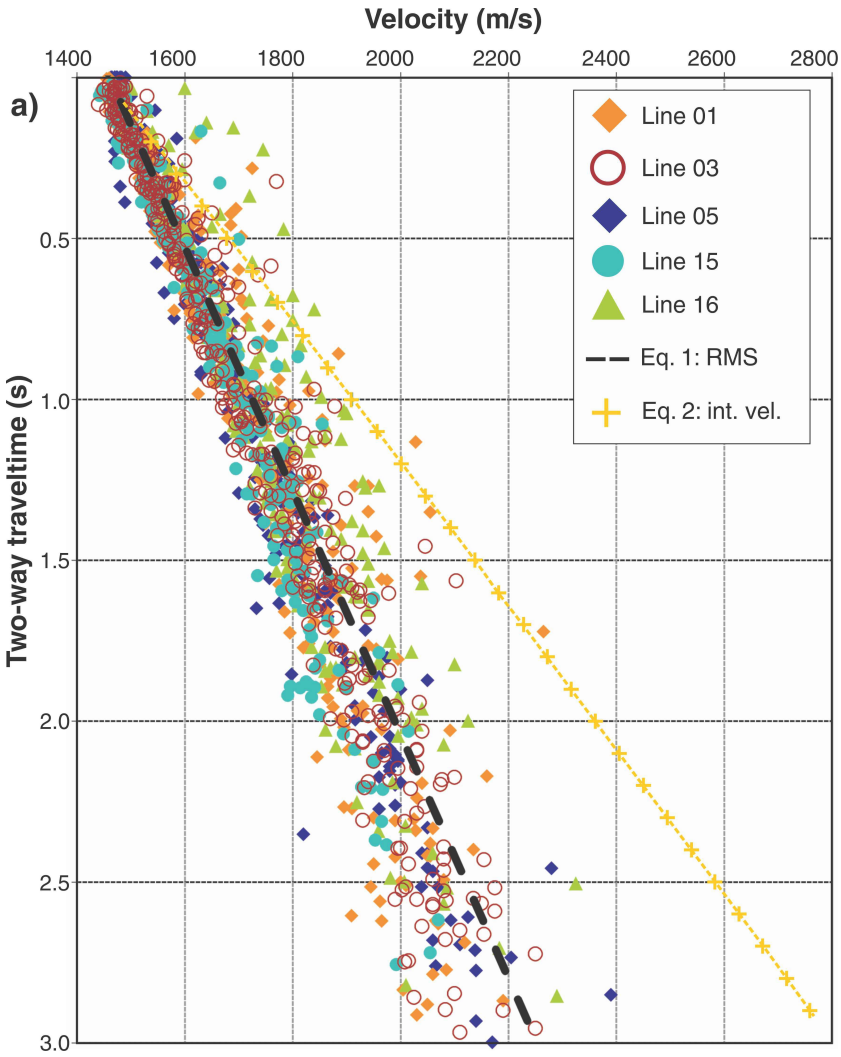

Figure 5. Root-mean-square (RMS) velocity values derived from multichannel seismic lines of ARA05C (determined every 100 common midpoint locations). **a)** Summary of all values as function of two-way traveltime below the seafloor from five multichannel seismic lines. A best-fit linear function (black solid line), using values down to a depth of 4 s two-way traveltime, was defined as average velocity-depth profile. From this, a linear trend of interval velocity (int. vel.) was determined (yellow crosses). Details for each line and deviations are shown in subsequent images. eq. = equation

Combining data from five seismic lines (14-01, 14-03, 14-05, 14-15, and 14-16) a best-fit linear root-mean-square velocity (V_{rms}) trend can be defined as:

$$V_{rms} = 0.242 \times T + 1465 \quad (1)$$

where T is the two-way traveltime in milliseconds below seafloor. A relatively high R^2 value of 0.92 shows the robustness of this trend.

This root-mean-square velocity trend is converted to interval velocity (V_{int}) following the method of Dix (1955) such that:

$$V_{int} = 0.4462 \times T + 1462.3 \quad (2)$$

Upper erosional unconformity

Deviations from this deep-water baseline were recognized at several locations across the study region. At the uppermost erosional unconformity, B, root-mean-square velocity values gradually increase underneath the erosional surface and then remain at the same velocity gradient as the deep-water trend (Fig. 5b) before gradually falling back to the deep-water trend. The zone of gradual root-mean-square velocity increase is 200–500 ms two-way traveltime thick. Three representative semblance plots for a deep-water setting, and two settings along the erosional unconformity from mid- and shallower water depths are shown in Figure 6a (*see* Fig. 4e for location of the common depth points along the seismic section). Along the entire seismic line 14-01, root-mean-square velocity values of the overlying postglacial sediments are either constant or show very little velocity increase with depth (1460–1475 m/s). This trend is observed along all lines analyzed crossing the slope region in the main study region, but is best defined along line 14-01.

Base of Shallow Bay sequence

The base of the Shallow Bay sequence was initially defined by Dietrich et al. (1989) as a prominent angular unconformity in the Mackenzie Trough and interpreted on the slope using amplitude character as the main indicator for the presence of this unconformity (Dietrich et al., 2010). Thus, the unconformity separates, in theory, older

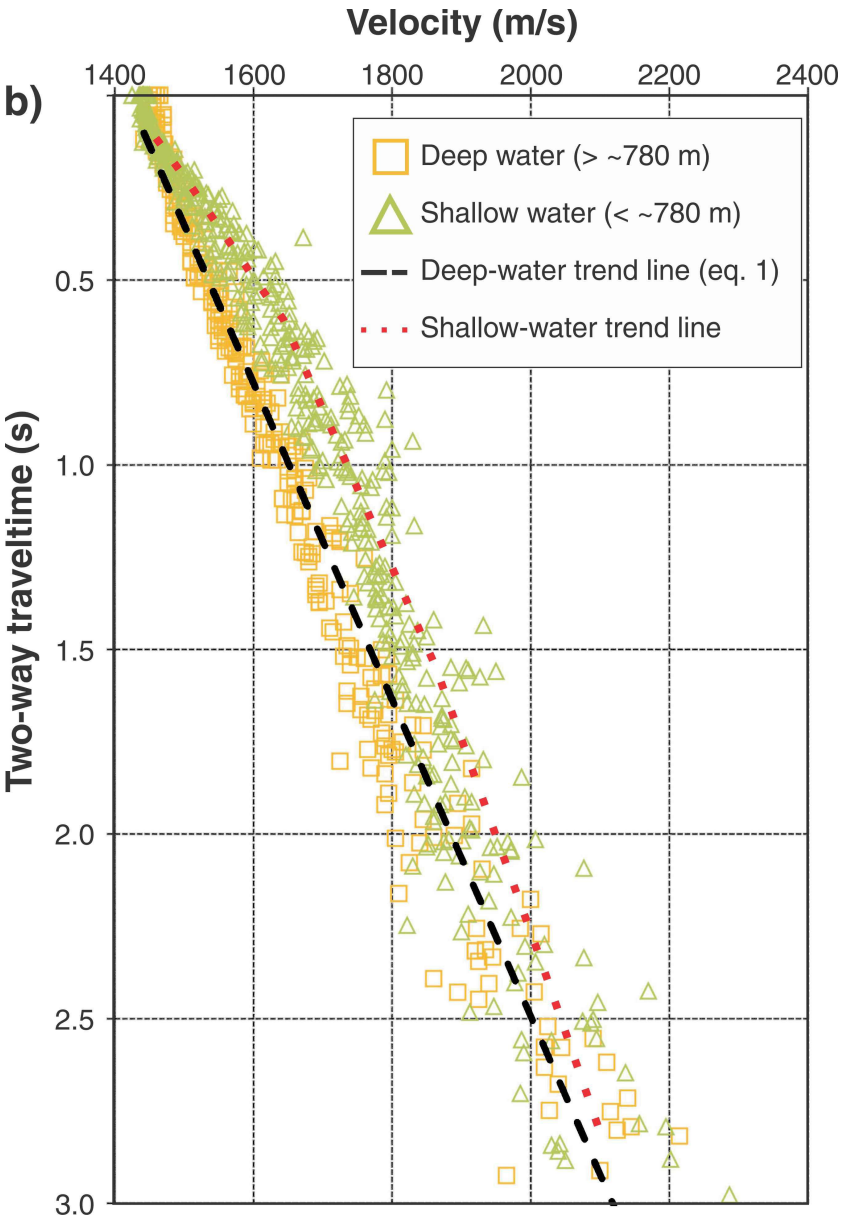

Figure 5. (cont.) b) The root-mean-square velocity values for multichannel seismic line 14-01. For comparison, the deep-water linear trend as defined by equation 1 is shown as black dashed line. A clear secondary trend with a higher velocity gradient is highlighted as a red dotted line. These higher root-mean-square velocities are associated with sediments beneath the uppermost erosional unconformity in shallow water (<~780 m). After the initial higher gradient, the velocities remain high and roughly parallel to the background trend. At greater depth (~1.75 s two-way traveltime), they start to gradually return to the background trend. *See* Figure 6a for three example semblance plots for further explanation of these velocity trends. eq. = equation

underlying strata from overlying younger or reworked material. The unconformity interpreted on the sections (yellow dashed line in Fig. 4a, 4b, 4d, and 4e) is one of many unconformities in the Kugmallit fan (K.M.M. Rohr, M. Riedel, and S.R. Dallimore, unpub. manuscript, 2016); it was interpreted because it is at a similar depth to the base of Shallow Bay sequence, interpreted tens of kilometres to the west (Dietrich et al., 2010). In principle, it would be expected that this boundary is associated with a velocity jump from lower values for the shallower lying strata to higher velocity values underneath.

The velocity analyses showed, however, that along the projected depth of this unconformity, the root-mean-square velocity trend only shows a change in gradient in shallower water (<500 m) as described above. The root-mean-square velocity gradient underneath the possible base of the Shallow Bay sequence is similar to the velocity gradient above as defined by equation 1, but the actual root-mean-square velocities are shifted to higher values (Fig. 6b, 6d). Above the unconformity is a steeper velocity gradient, likely an effect of the overlying unconformity. No difference in the root-mean-square velocity gradient is seen in deeper water across the base of this unconformity.

Channel-levée sequences

Discontinuities in root-mean-square velocity can be correlated with lithological boundaries within channel-levée sequences described in recent work by K.M.M. Rohr and co-workers (K.M.M. Rohr, M. Riedel, and S.R. Dallimore, unpub. manuscript, 2016). Fine-grained (low-reflectivity) muds of a levée (Fig. 6b) separate a zone of high gradient from

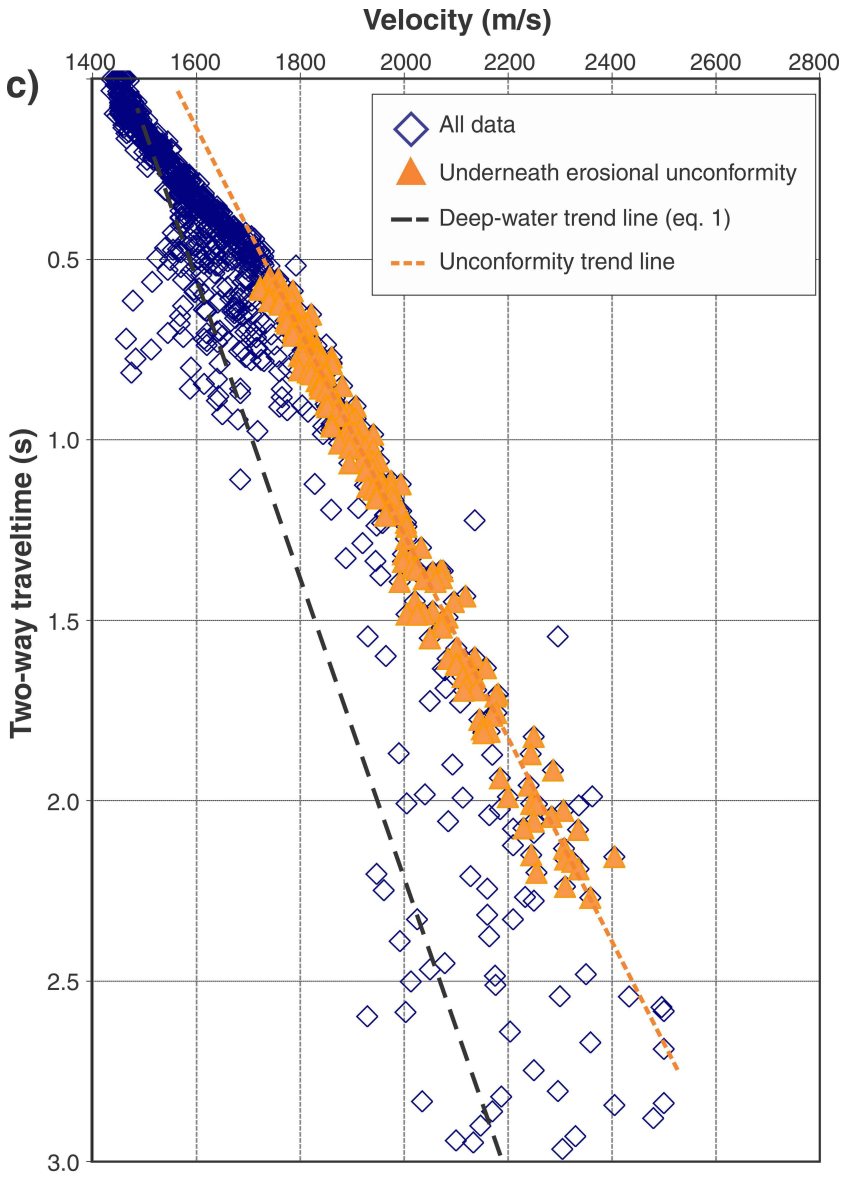

Figure 5. (cont.) c) Root-mean-square velocity values for multichannel seismic line 14-19. For comparison, the deep-water linear trend as defined by equation 1 is shown as a black dashed line. The orange dashed line is the best-fit linear trend through the velocity data points underneath the erosional unconformity (orange triangles). Projecting the velocity trend underneath the unconformity to the background yields a depth difference of equivalent about 0.5 s two-way traveltime (~425 m using a velocity of 1700 m/s); however, this depth difference is not necessarily the amount of overburden removed, as differential compaction influences the velocity trends and needs to be taken into account for determining the amount of erosion. eq. = equation

a zone of normal gradient, but higher values on line 14-03. Erosional unconformities within this sequence have removed up to 400 m of section and may have contributed to creation of discontinuities.

Channel-fill sequence

Along seismic line 14-03 (Fig. 4f), a channel complex is intersected, slightly further northwest from the Pokak fluid-expulsion feature. A low-velocity zone along a deeper channel-fill sequence also has been identified by Rohr and co-workers (K.M.M. Rohr, M. Riedel, and S.R. Dallimore, unpub. manuscript, 2016), using the 3-D seismic velocity data volume, with velocities defined through prestack Kirchoff time-migration. The RV *Araon* multichannel seismic data confirm the interpretation by Rohr and co-workers (K.M.M. Rohr, M. Riedel, and S.R. Dallimore, unpub. manuscript, 2016) of the occurrence of low-velocity zones associated with channel-fill deposits. The low velocity is bound to the high-reflectivity zone of the channel fill itself and not the surrounding levée complexes. Thus, the channel fill is likely coarser grained (but fluid-filled) sand, whereas the levée complexes consist of finer grained silt to mud-dominated sediments.

420 m fluid-expulsion feature

A flat-topped fluid-expulsion feature at a water depth of 420 m has been the site of increased scientific activity during multiple expeditions in the past, and work conducted at this site include sediment coring for measuring pore-fluid geochemistry (Paull et al., 2015), temperature measurements (Riedel et al., 2015b), detailed seafloor imaging with a remotely operated vehicle and high-resolution bathymetric

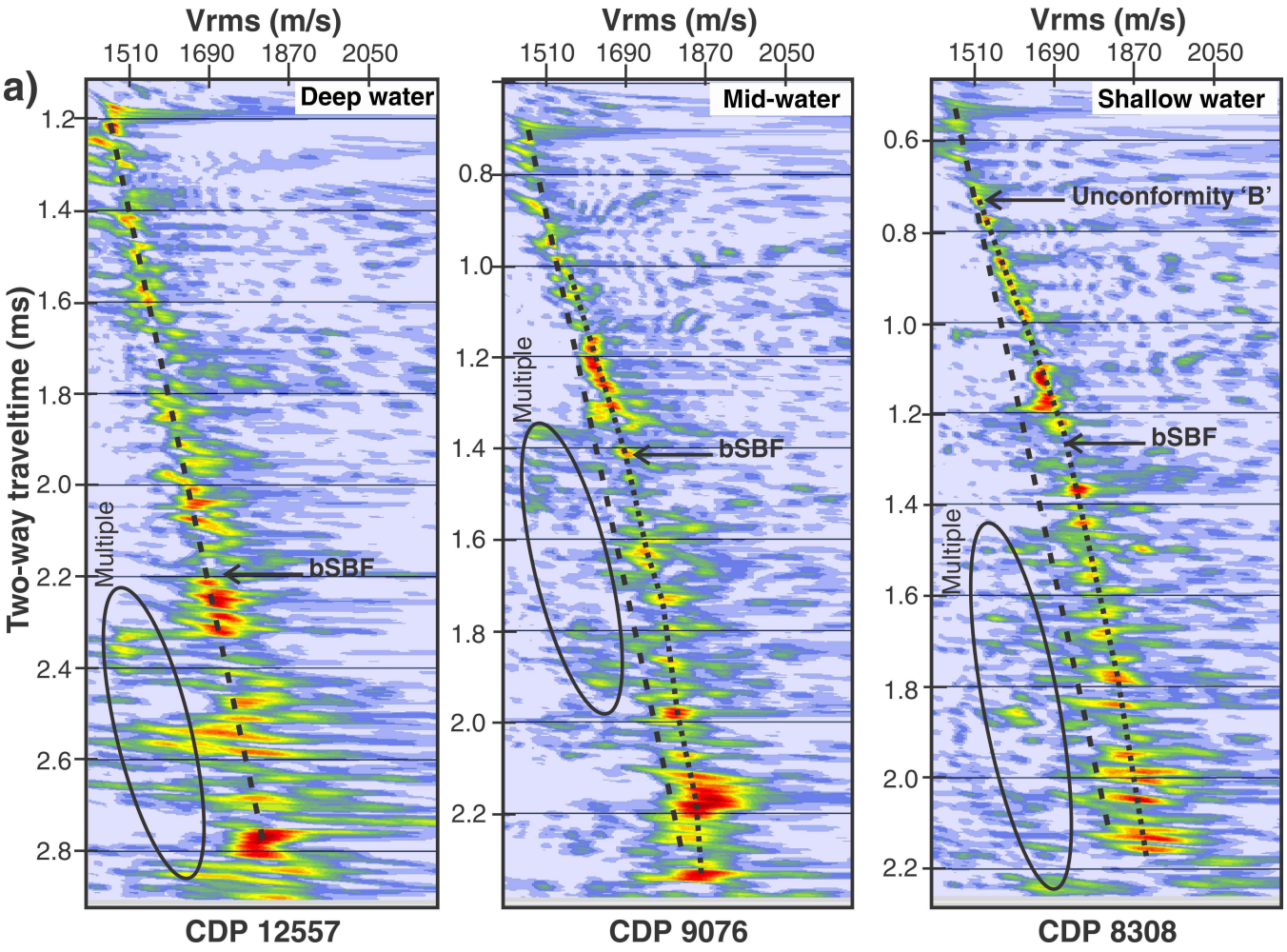

Figure 6. Velocity semblance plots at common depth points of multichannel lines shown in Figure 4. **a)** Multichannel seismic line 14-01; left: CDP 12557, defining the deep-water baseline trend; centre: CDP 9076 at mid-water depth location, showing a deviation from the baseline starting at 1.1 s two-way traveltime, beneath the erosional unconformity 'B'; and right: CDP 8308 at the shallow-water portion of the line with a clear separation of velocities from the baseline trend starting at about 0.2 s two-way traveltime below the uppermost erosional unconformity (bSBF = base of Shallow Bay sequence, CDP = common depth point).

mapping with an autonomous underwater vehicle (Paull et al., 2015), as well as imaging of gas flares in the water column (Jin et al., 2015).

Seismically, the 420 m fluid-expulsion feature is marked by a strong seafloor return at the centre from the occurrence of shallow free gas (Fig. 4d). Imaging beneath the structure is completely masked by the free-gas occurrence. To both sides of the fluid-expulsion feature, an apron of sediments is seen forming a wedge of interbedded mud flows and regular (hemipelagic) sediments. A series of five semblance plots show the evolution of the root-mean-square velocity through the entire fluid-expulsion feature (Fig. 6c). At the southern rim of the feature within the apron of interbedded mud flows and regular sediments (CDP 9120), the root-mean-square velocity increases with depth following the baseline gradient as sediments do not contain any free gas. The next location at the southern rim, but within the flat-top portion of the fluid-expulsion feature (CDP 9185) shows the effect of free gas, as root-mean-square velocity for few horizons can be identified, but mostly at velocities around 1460 m/s, much lower than the baseline. Near the seafloor, diffractions with a nonhyperbolic moveout interfere with regular reflections, so that semblance highs are at much lower velocity values. This effect is amplified in the centre of the fluid-expulsion feature (CDP 9260). The top 400 ms two-way traveltime shows only diffractions and no primary energy can be mapped. The multiple reflections show less interference from diffractions. Across the northwestern rim of the fluid-expulsion feature (CDP 9335), some primary energy can be seen as semblance highs, but velocities are lower than the baseline, again indicating the presence of some free gas. The final location at the northwestern apron of interbedded mud flows with regular sediments (CDP 9400) shows that the root-mean-square velocities are fully recovered and again increase with depth following the baseline trend.

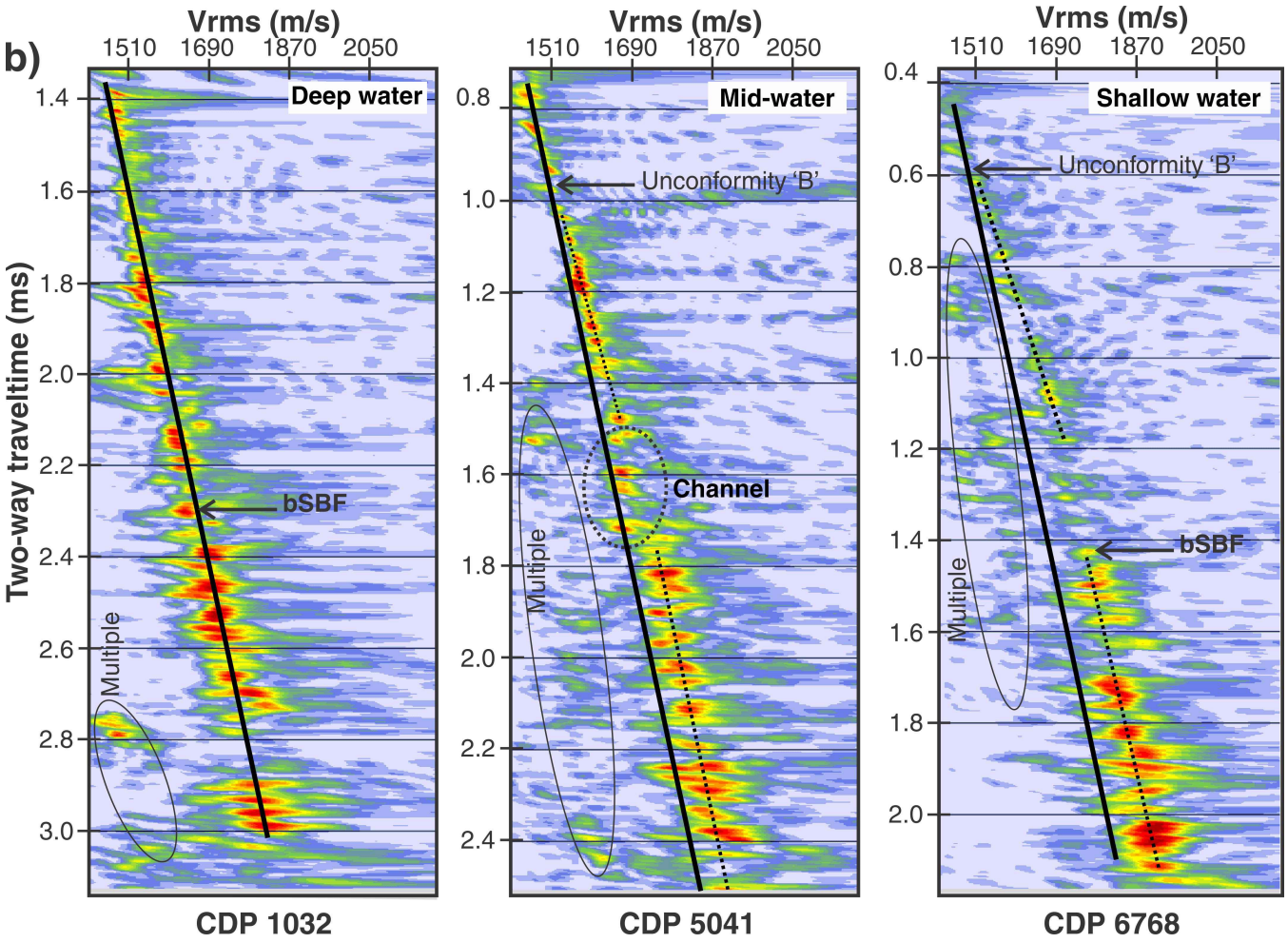

Figure 6. (cont.) b) Multichannel seismic line 14-03; left: CDP 1032, defining the deep-water baseline trend; centre: CDP 5041 at mid-water depth location showing a deviation from the baseline starting at 1.1 s two-way traveltime, beneath the erosional unconformity 'B' as well as a low-velocity zone associated with channel sands; and right: CDP 6768 at the shallow-water portion of the line with a clear separation of velocities from the baseline trend starting at about 0.2 s two-way traveltime below the uppermost erosional unconformity (bSBF = possible base of Shallow Bay sequence, unconformity interpreted as yellow dashed line in Fig. 4; CDP = common depth point).

The semblance-based root-mean-square velocities can be used to convert the time-migrated section to depth. As mentioned by Rohr and co-workers (K.M.M. Rohr, M. Riedel, and S.R. Dallimore, unpub. manuscript, 2016), the 420 m fluid-expulsion feature is linked to an underlying anticline, which is part of a regional fold-and-thrust belt, trending from the northwest at about 110° (measured from geographic north). The depth to the anticline is approximately 3 km (Fig. 4d).

760 m fluid-expulsion feature (triple mound)

Along multichannel seismic line 14-15, a fluid-expulsion feature at 760 m water depth is imaged. This fluid-expulsion feature is characterized by three individual mounds. Two of those are flat-top features such as the 420 m fluid-expulsion feature, but the third is a conical mound, almost symmetrical in shape (Paull et al., 2015). At four locations, semblance velocity analyses show the trend of the root-mean-square velocity across this triple-mound feature (Fig. 6e). At the southern rim, just northwest of the rim of extensional normal faults, the root-mean-square velocity values follow the overall deep-water baseline trend. At the second location, inside the central depression of the mound features, the uppermost root-mean-square velocity values are below the baseline trend, but above seawater velocity (~1460 m/s), but some interference from diffractions are also seen. Close to the flat-top mound, the velocities are all significantly smaller than the baseline trend and recover to the baseline only at depths of about 1.6 s two-way traveltime, about 500 ms two-way traveltime, equivalent to about 400 m below seafloor. Near the north cone feature, velocities are again along the baseline trend. Overall, the semblance analyses conducted along the line through the triple-mound fluid-expulsion

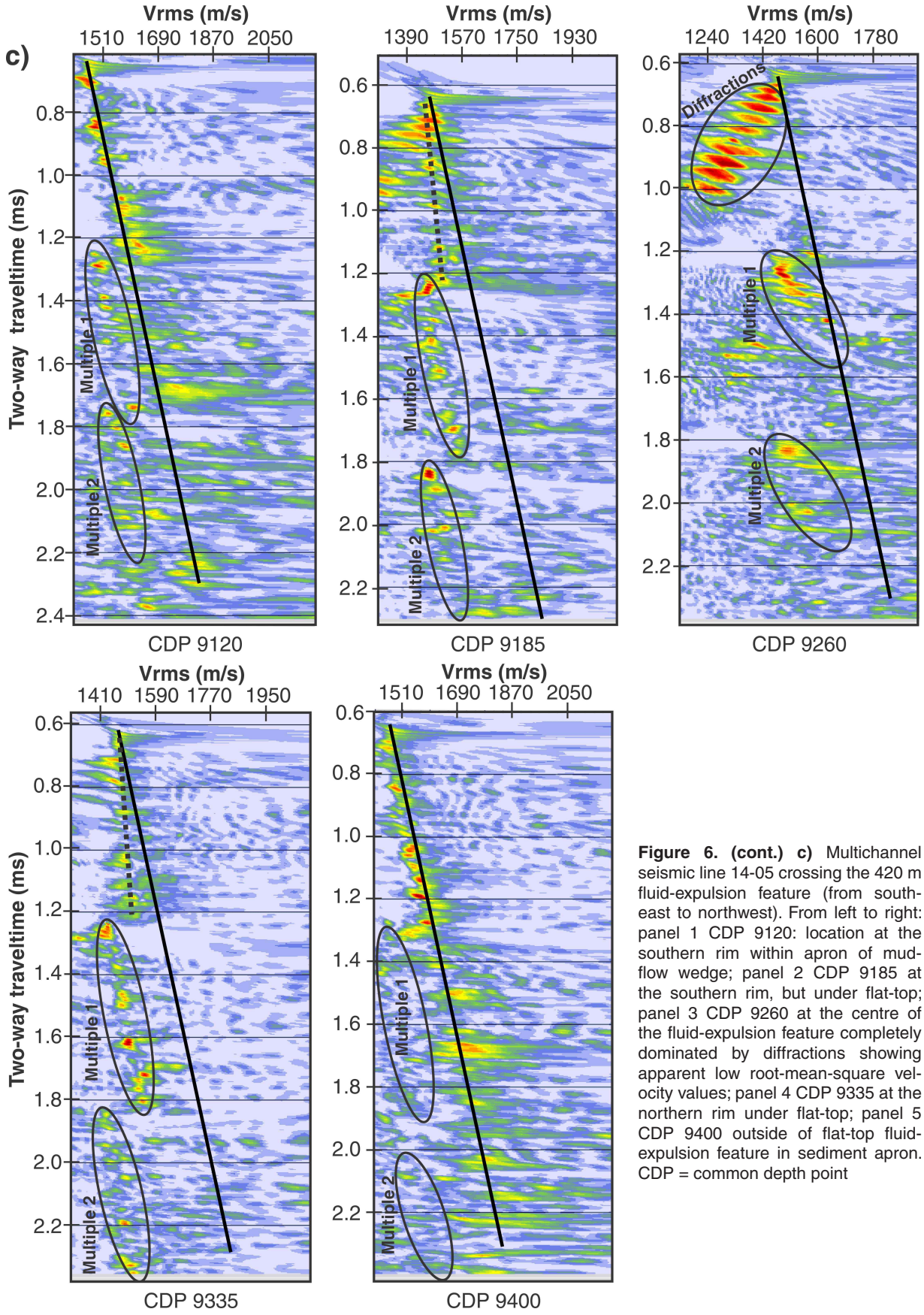

Figure 6. (cont.) c) Multichannel seismic line 14-05 crossing the 420 m fluid-expulsion feature (from south-east to northwest). From left to right: panel 1 CDP 9120: location at the southern rim within apron of mud-flow wedge; panel 2 CDP 9185 at the southern rim, but under flat-top; panel 3 CDP 9260 at the centre of the fluid-expulsion feature completely dominated by diffractions showing apparent low root-mean-square velocity values; panel 4 CDP 9335 at the northern rim under flat-top; panel 5 CDP 9400 outside of flat-top fluid-expulsion feature in sediment apron. CDP = common depth point

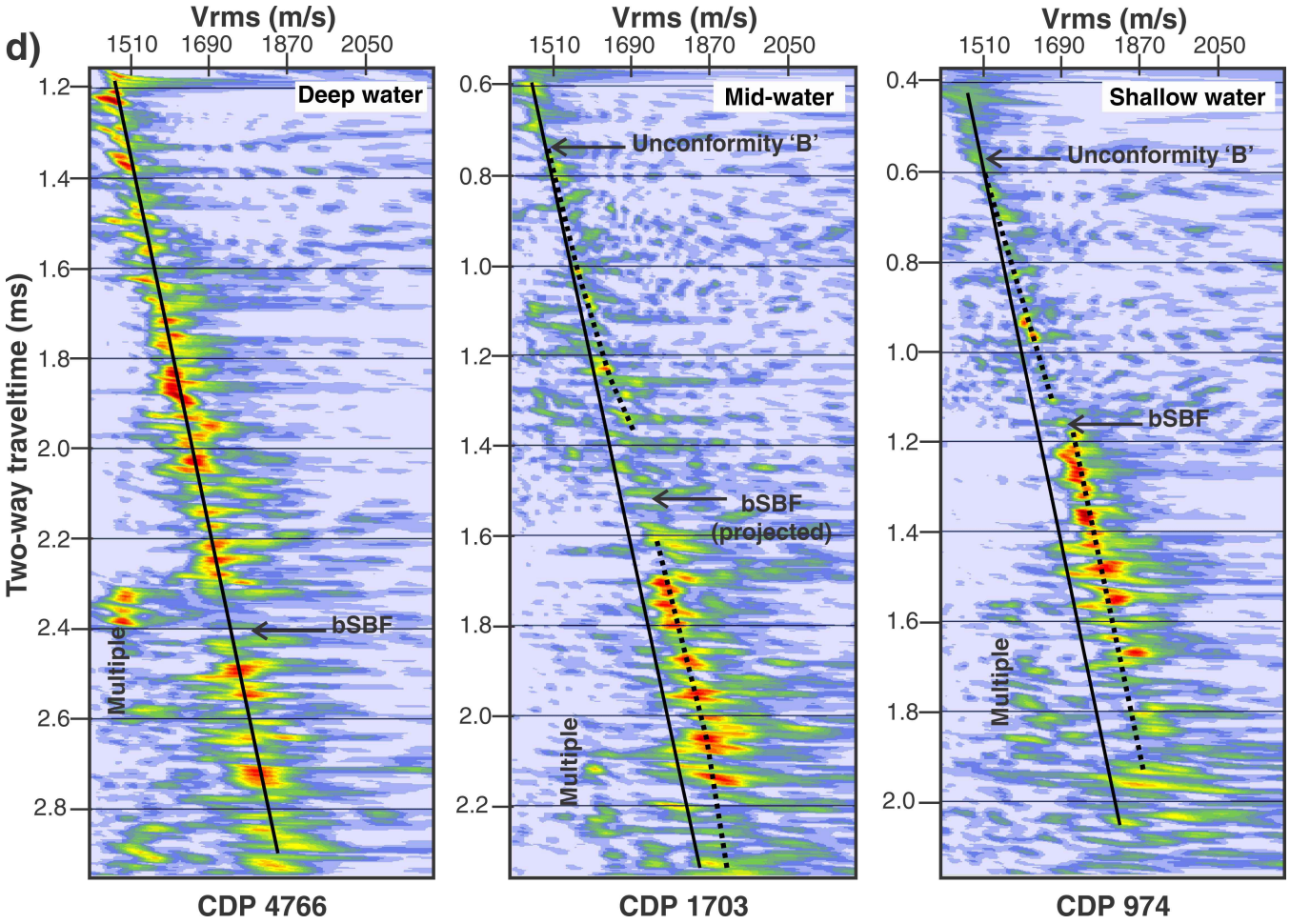

Figure 6. (cont.) d) Multichannel seismic line 14-15, highlighting the velocity trend associated with the uppermost erosional unconformity 'B' (bSBF = possible base of Shallow Bay sequence, unconformity interpreted as yellow dashed line in Fig. 4). Locations of these common depth points (CDPs) are shown in Figure 4a.

feature appear to not show any evidence for the presence of free gas, as root-mean-square velocities are never below that of seawater. The lower than baseline root-mean-square velocity values suggest a fluid-rich nature of the mud extruded at these features; however, as the line is not crossing over the centre of any of the three orifices, the presence of free gas at those central locations cannot be ruled out.

Mackenzie Trough unconformity

The Mackenzie Trough region has recently been studied for evidence of glacial erosion and deposition of till material using a dense grid of 2-D multichannel seismic lines provided by an industry partner (Batchelor et al., 2013a, b). In this region, several multichannel seismic lines were acquired during the ARA05C expedition in 2014 (Fig. 2b). The seismic structure is dominated by the occurrence of an erosional unconformity from glacial erosion during ice advance (Fig. 4g). Sediments underneath the erosional unconformity are tilted and strongly faulted, whereas sediments above are semiparallel to the unconformity and seafloor. These sediments are synglacial deposits such as moraine-type and/or till-type sediments with a mixture of grain sizes. It is interesting to note that a postglacial layer (or drape) of well laminated sediments cover the synglacial deposits. Careful semblance velocity analyses showed a very different velocity trend in the Mackenzie Trough region than the eastern portion of the study zone (Fig. 5c, 6f, 6g); the first difference is in the much higher root-mean-square velocity values and velocity gradient than what is observed at similar depths in the deeper water portion of the eastern study region. The drape of postglacial sediments is almost at a constant, near-water root-mean-square velocity (1460–1470 m/s). The underlying till or moraine-type sediment show a fast increase in root-mean-square velocity up to the erosional unconformity. This velocity gradient is the highest observed gradient along all of the RV *Araon* multichannel seismic data acquired in 2013 and 2014. Earlier interpretations by Blasco et al. (2013) and Batchelor et al. (2013a) suggested that these sediments are glacial till and/or sand-rich (water-saturated) sediments. In comparison, sand-rich channels at equivalent or slightly deeper burial depths intersected further

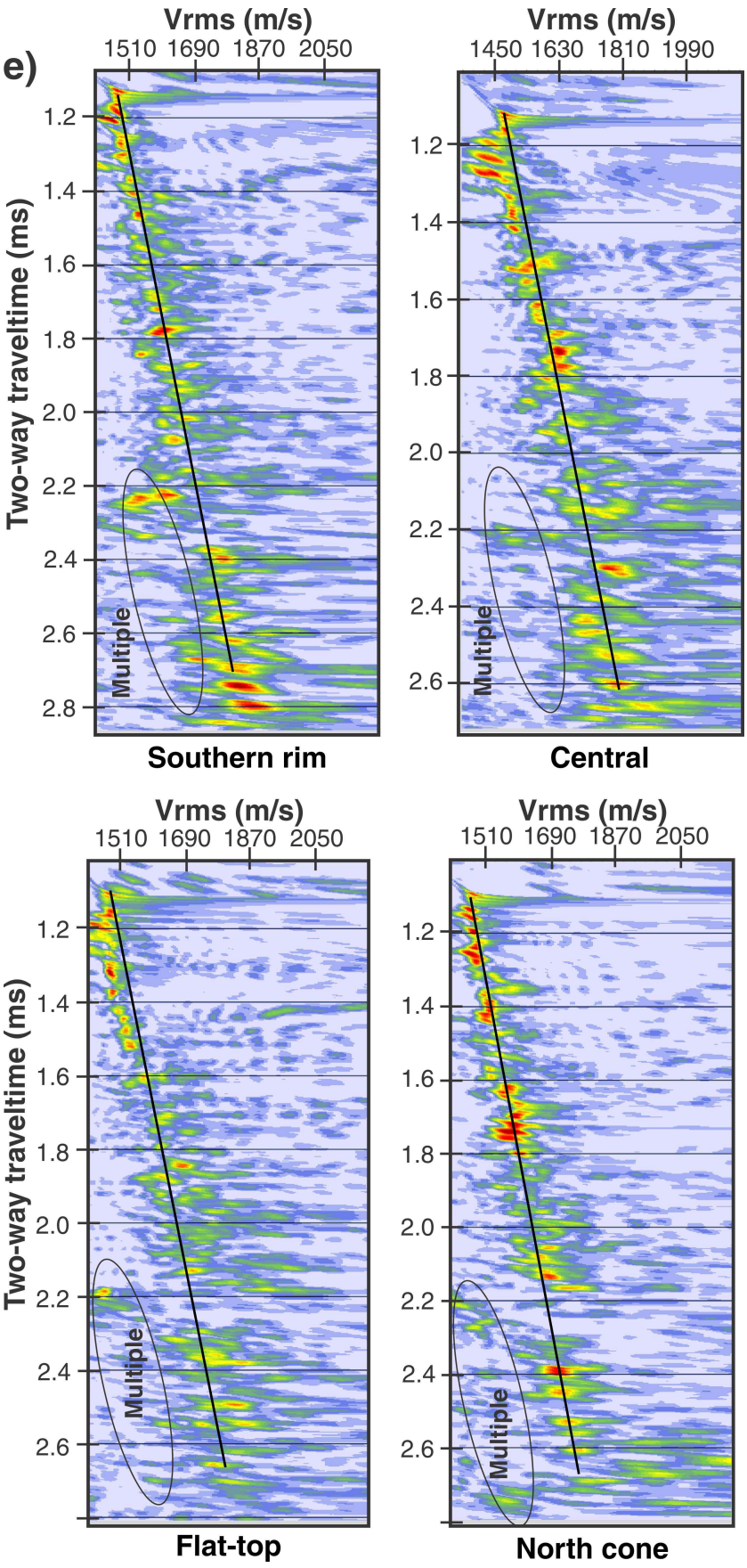

Figure 6. (cont.) e) Multichannel seismic line 14-15, highlighting the velocity trends associated with the 760 m fluid-expulsion feature. Locations of these common depth points (CDPs) are shown in Figure 4a.

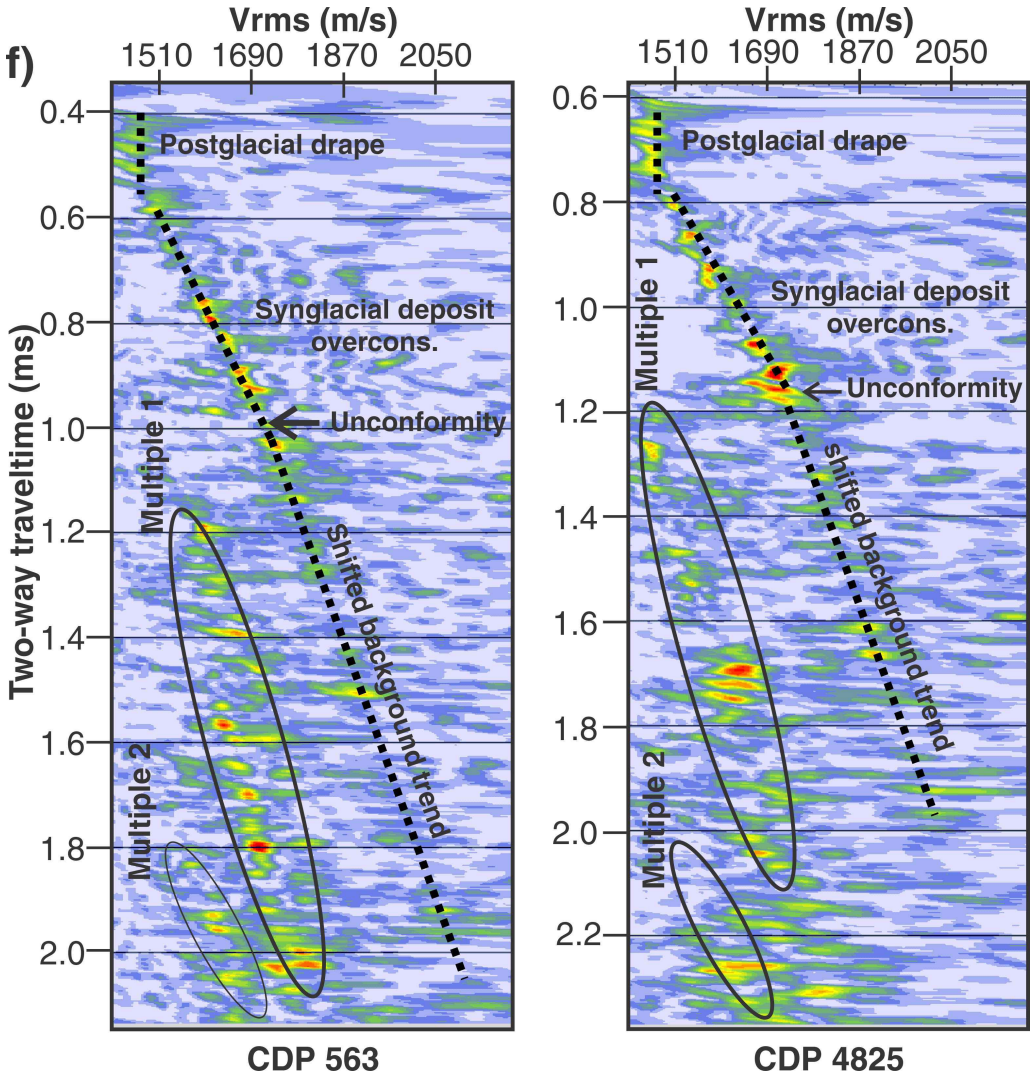

Figure 6. (cont.) f) Two common depth points (CDPs) from multichannel seismic line 14-19 (left: CDP 563; right: CDP 4825), highlighting the velocity trends associated with the glacial erosion and apparent overconsolidation (over-cons.) of the synglacial deposits. Locations of these CDPs are shown in Figure 4g.

east of the Beaufort Sea margin show lower than average root-mean-square velocity values e.g. along line 14-03 (Fig. 6b) and as shown by Rohr and co-workers (K.M.M. Rohr, M. Riedel, and S.R. Dallimore, unpub. manuscript, 2016). The unusually high velocity gradient with the Mackenzie Trough region could therefore be a result of an apparent overconsolidation of the sediment from the glacial ice load. Sediments underneath the unconformity itself reveal a velocity gradient that is similar to the background deep-water velocity trend as defined by equation 1. No effect of overconsolidation is invoked for these deeper sediments as the velocity gradient appears simply shifted to higher values. Overconsolidation would possibly become less strong with depth and thus a curved velocity-depth profile toward the deep-water trend is expected in such a case. Since the velocity gradient appears rather constant, but shifted to overall higher values below the unconformity, this shift is interpreted as a result of erosion of the overburden. Projecting the velocity trend below the unconformity onto the deep-water background trend suggests a missing overburden of up to 0.5 s (two-way traveltime). Using a velocity of 1700 m/s, this is equivalent to a depth of about 425 m; however, this is not necessarily the amount of overburden removed by erosion, as differential compaction from the glacial history in the Mackenzie Trough needs to be taken into account.

A second unique observation along multichannel seismic lines 14-19 (Fig. 4g) and 14-20 (Fig. 4h) is the potential onset of a marine gas-hydrate stability zone and the occurrence of a bottom-simulating reflector. In water depths exceeding about 750 m, the seismic data along lines 14-19 and 14-20 show a bright reflection at a two-way traveltime of about 390 ms below seafloor. This reflection

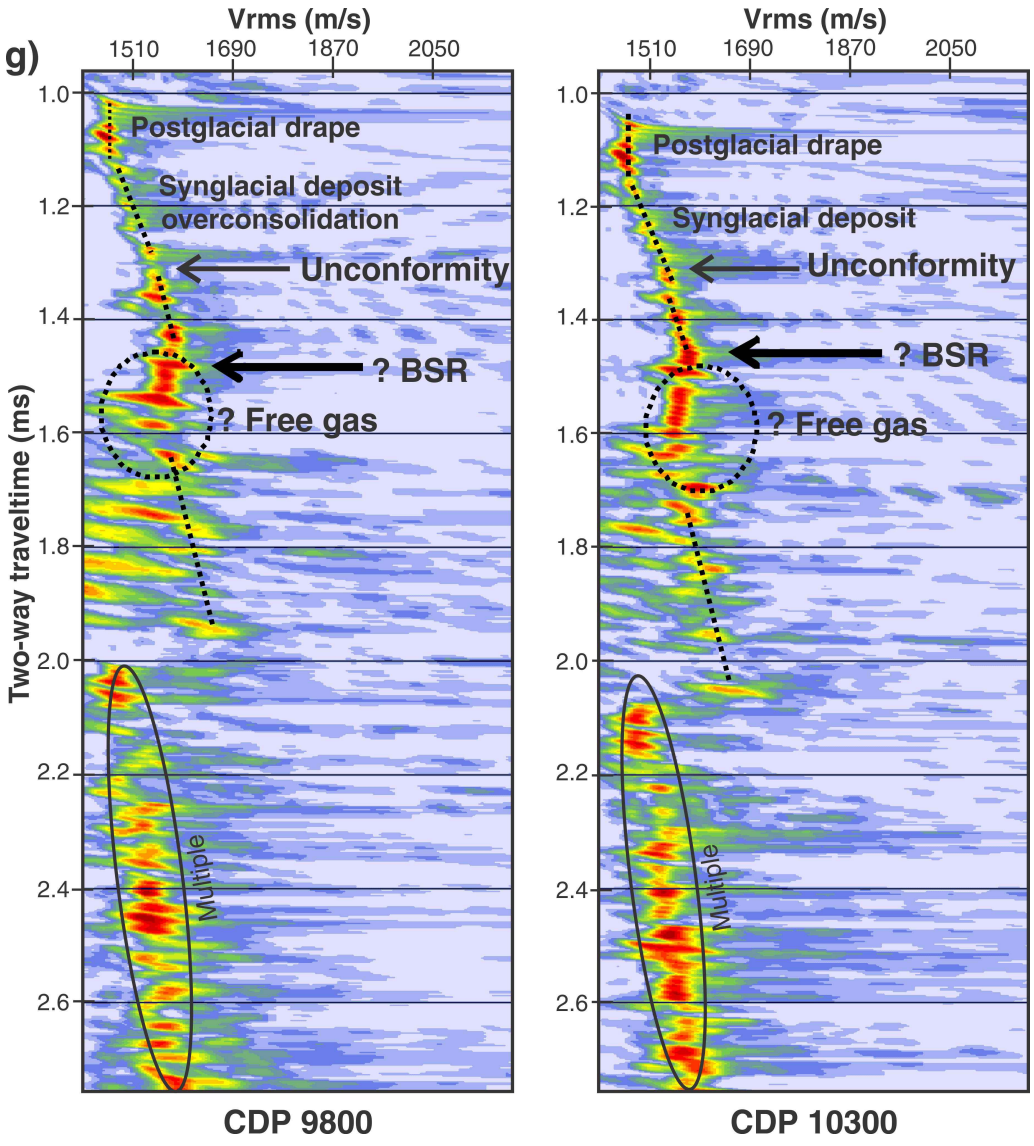

Figure 6. (cont.) g) Two common depth points (CDPs) from multichannel seismic line 14-19 (left: CDP 9800, right: CDP 10800), highlighting the velocity trends associated with the potential occurrence of a gas-hydrate stability zone and bottom-simulating reflector (BSR); locations of these CDPs are shown in Figure 4g.

is associated with a relatively thick low root-mean-square velocity zone (Fig. 6g), suggesting the presence of some free gas. Nowhere else along any of the multichannel seismic lines does such strong root-mean-square velocity reduction (with the exception of the fluid-expulsion features) coupled with a bottom-simulating reflector–like event exist; however, as indicated in Figure 4h, the bottom-simulating reflector–like event lacks some characteristics usually attributed to a gas-hydrate phase boundary. The bottom-simulating reflector–like event seen is not truly crosscutting regular stratigraphy, but rather appears similar in nature to an erosional unconformity: high-amplitude reflections terminate at the bottom-simulating reflector–like event. Additional seismic sections are required, especially acquired in an orthogonal direction, to verify the nature of this event, coupled with dedicated heat-flow measurements to constrain the temperature regime. A shelf-related bottom-simulating reflector was identified from the industry 3-D seismic data (Riedel et al., 2015a), but no velocity information was available from the 3-D data to identify possible free-gas occurrences beneath the base of gas-hydrate stability.

AMPLITUDE-VERSUS-OFFSET PROCESSING

The multichannel seismic data acquired with the approximately 1500 m long streamer allows utilizing prestack analyses techniques, such as amplitude-versus-offset processing. The useable range of angle of incidence is

a function of water and subseafloor depths and the velocity of the sediments. The amplitude-versus-offset processing trend is often applied by using approximations to the complex Zoeppritz equations (Zoeppritz, 1919), such as the one suggested by Shuey (1985), which considers angles of incidence less than 35° to 40°. Commonly, the amplitude-versus-offset processing response is then further simplified and graphically displayed by using intercept (vertical incidence reflection coefficient) and gradient values (e.g. Castagna and Swan, 1997). With the offsets available from the RV *Araon* multichannel seismic data, the range in angles available for amplitude-versus-offset processing work is sufficient up to a water depth of about 2000 m (maximum angle of incidence at seafloor ~20°); however, in shallow water across the shelf, the critical angle of incidence may be reached at relatively short offsets, if the velocity contrast between overlying water and seafloor sediments is large (e.g. in the presence of permafrost). Postcritical reflections and refracted arrivals therefore make processing and analyses of the multichannel seismic data more challenging.

Amplitude-versus-offset processing analyses can be used to address multiple questions involving geohazard analyses, as amplitude-versus-offset processing can provide estimates on the sediment shear-wave (S-wave) velocity, pore-fluid filling, and density (Ariffin et al., 1995). In this approach, the reflection coefficients as function of angle of incidence (or offset) show a different trend for normally consolidated sediments compared to those that are overpressured (e.g. Miley and Kessinger, 1999; Dutta, 2002; Dash et al., 2004). All elastic properties (P- and S-wave velocities and density) are significantly altered by the increase in pore pressure (e.g. Dvorkin et al., 1999). Prior to conducting the amplitude-versus-offset processing analyses, a comparison of far-offset and near-offset stack is useful to identify potential anomalies. According to the predicted amplitude-versus-offset processing response of normally consolidated, brine-saturated sediments, the far-offset stack should be higher in amplitude than a near-offset stack (Ariffin et al., 1995). If abnormal pressures or fluid content are at play, this may no longer be the case and thus, a difference plot between near- and far-offset stacks may indicate potential zones of overpressure. These can then be investigated with more detailed amplitude-versus-offset processing analyses, or combined with full wave-form inversion (e.g. Dutta, 2002). In this simple processing step, data should be corrected at a minimum for spherical divergence. Changes in the shape of the wave form from e.g. frequency loss occurring at far offsets could generate a poor signal-to-noise ratio in this simple approach. Therefore, the difference in near-offset to far-offset stack is only a quick approach to identify regions of interest.

The authors have used a portion of multichannel seismic line 14-05 to demonstrate the difference-plot technique to identify possible anomalous amplitude-versus-offset processing intervals (Fig. 7). The difference between near- and far-offset stacks shows, for the most part, a normal amplitude-versus-offset processing response where the far-offset stack is higher in amplitude than the near-offset stack. An anomalous interval is seen at a depth of about 0.8 s to 1.0 s two-way traveltime between common depth points 100–700. Here, the far-offset stack is lower in amplitude than the near-offset stack, suggesting possible anomalous subsurface conditions (e.g. presence of free gas and/or overpressure). The 420 m fluid-expulsion features itself is gas-charged (and gas is seen venting from the surface), creating acoustic masking underneath with no coherent signal to be recovered.

SUMMARY AND GEOHAZARD IMPLICATIONS

The set of multichannel seismic lines acquired in the southern Beaufort Sea with the IBRV RV *Araon* helps assess potential geohazards in the region and provides an excellent opportunity to verify velocity trends observed in the industry 3-D seismic data (K.M.M. Rohr, M. Riedel, and S.R. Dallimore, unpub. manuscript, 2016) by tying velocity values to individual reflections or reflector packages. The multichannel seismic data also extends beyond the limits of the two 3-D seismic volumes and brackets the transition from shelf-dominated processes with relict permafrost to the deep-water traditional marine environment.

Initial processing of these multichannel seismic lines revealed a complex set of structural settings that were already previously identified as regional geohazards:

- Localized fluid-expulsion features or mud volcanoes with active fluid, gas, and mudflows to the surface, that are linked to possible overpressure zone at greater depth; and
- Sand-filled channel sequences with extensive levée systems that are prone to large-scale failure.

The multichannel seismic data also revealed previously unrecognized features:

- Occurrence of an erosional unconformity with a distinct velocity trend indicating erosion in the Mackenzie Trough region; the unconformity marks a sudden step in physical properties of the sediments that should be taken into account in further assessments of geohazards; and
- Occurrence of a deep-water marine gas-hydrate stability zone with the presence of free-gas accumulation underneath a bottom-simulating reflector in the Mackenzie Trough region (compare also to Riedel et al., 2015a).

Further to the recognition of free gas associated with the major fluid-expulsion zones known to occur on the Beaufort slope region, the multichannel seismic data allowed processing of the data to greater depths, beyond what is provided by the 3-D industry seismic data, and thus link the expulsion zones to the underlying tectonic structures.

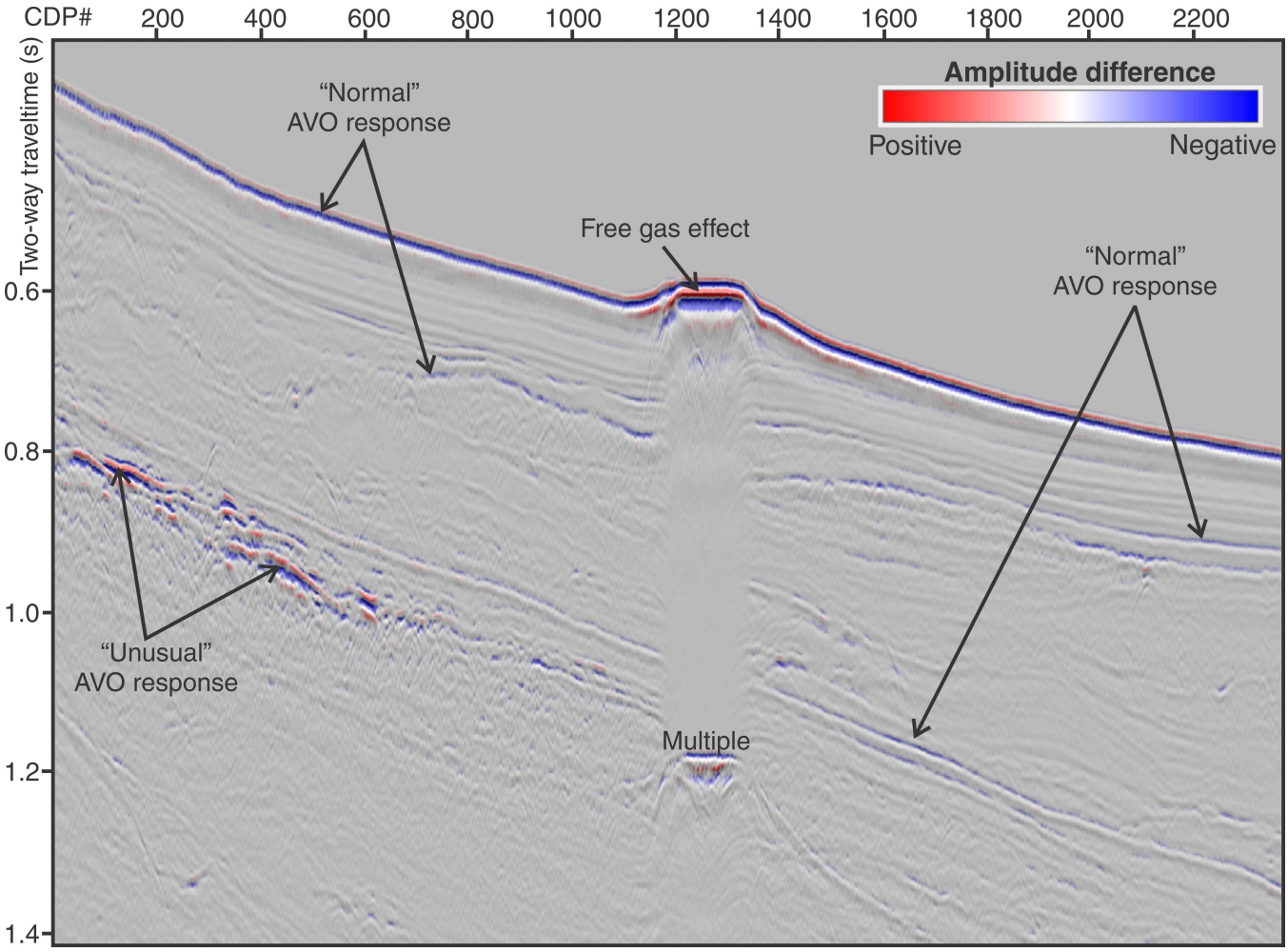

Figure 7. Section of multichannel seismic line 14-5 from ARA05C (Jin and Dallimore, 2016), showing an overlay of the regular stack (grey scale) and difference plot of near- and far-offset stack. The blue colours represent "normal" amplitude-versus-offset (AVO) response, where the far-offset stack is higher in amplitude than the near-offset stack. Note the progressive shift in AVO response in the seafloor from a broadening of the seafloor reflection (either an effect of decreasing frequency content in far offset data, or a softening of the seafloor reflection coefficient as a result of an increase in the thickness of a mud-dominated drape). An "unusual" AVO response, where the far-offset data are equal or similar in amplitude than the near-offset data is seen along the line below 0.8 s two-way traveltime, possibly associated with the occurrence of some free gas. CDP = common depth point

All major expulsion features imaged by the RV *Araon* multichannel seismic data can be traced to an underlying anticline, suggesting significant overpressure buildup in these folded structures. The source of fluid (and mud) can be placed at depths of about 1.8 km (760 m), 3.0 km (420 m), and 3.0 km (Pokak fluid-expulsion feature).

Combining the new 3-D data interpretation available (K.M.M. Rohr, M. Riedel, and S.R. Dallimore, unpub. manuscript, 2016) and work by Batchelor et al. (2013a) in the Mackenzie Trough, with the velocity trends defined from the RV *Araon* multichannel seismic data, it becomes evident that the Shallow Bay sequence boundary cannot easily be defined for most of the Beaufort slope region east of the Mackenzie Trough using the same arguments as Dietrich et al. (2010). The RV *Araon* data as well as the 3-D data show no clear (or single) unconformity that can be assigned as the base of the Shallow Bay sequence. Instead, numerous erosional events, often rugged in nature and changing significantly across the region are seen; they are attributed to a dynamic sediment-depositional environment of channel and levée complexes.

OUTLOOK FOR FUTURE WORK

To support the development of the International Ocean Discovery Program preproposal (Paull et al., 2012) into a "full proposal", the RV *Araon* 2-D multichannel seismic data will need additional processing, particularly across the shelf to enhance structural imaging and velocity determination.

The above-outlined processing scheme will need to be modified to address challenges with shallow-water multiples as well as fast-changing velocity contrasts within the upper 500–800 m below seafloor.

As the deep-water portion of the data are currently well processed and imaged with good recovery of velocity functions and true-amplitude nature of the data preserved, the effort should focus on the shelf and upper slope region. Improved imaging and true-amplitude processing of the shallow data set will support the full proposal to pass the critical review by International Ocean Discovery Program, particularly the drilling safety and environmental assessments.

ACKNOWLEDGMENTS

The authors would like to thank the onboard Korea Polar Research Institute science and technical team for data acquisition and initial processing. Additional thanks go to M. Duchesne for a careful and thoughtful review of the manuscript.

REFERENCES

Ariffin, T., Solomon, G., Ujang, S., Bee, M., Jenkins, S., Corbett, C., Dorn, G., Withers, R., Özdemir, H., and Pearse, C., 1995. Seismic tools for reservoir management, Oilfield Review, Issue Winter 1995, p. 4–17. <https://www.slb.com/~/media/Files/resources/oilfield_review/ors95/win95/12950417.pdf> [accessed March 15, 2016]

Batchelor, C.L., Dowdeswell, J.A., and Peitras, J.T., 2013a. Seismic stratigraphy, sedimentary architecture and palaeo-glaciology of the Mackenzie Trough: evidence for two Quaternary ice advances and limited fan development on the western Canadian Beaufort Sea margin; Quaternary Science Reviews, v. 65, p. 73–87. doi:10.1016/j.quascirev.2013.01.021

Batchelor, C.L., Dowdeswell, J.A., and Peitras, J.T., 2013b. Variable history of Quaternary ice-sheet advance across the Beaufort Sea margin, Arctic Canada; Geology, v. 41, p. 131–134. doi:10.1130/G33669.1

Blasco, S., Bennett, R., Brent, T., Burton, M., Campbell, P., Carr, E., Covill, R., Dallimore, S., Davies, E., Hughes-Clarke, J., Issler, D., Leonard, L., MacKillop, K., Mazzotti, S., Patton, E., Rogers, G., Shearer, J., and White, M., 2013. 2010 State of knowledge: Beaufort Sea seabed geohazards associated with offshore hydrocarbon development; Geological Survey of Canada, Open File 6989, 340 p. doi:10.4095/292616

Brigham, J.K. and Miller, G.H., 1983. Paleo-temperature estimates of the Alaskan Arctic Coastal Plain during the last 125,000 years; *in* Proceedings of the 4th International Conference on Permafrost, Fairbanks, Alaska, p. 80–85.

Castagna, J.P. and Swan, H.W., 1997. Principles of AVO crossplotting; The Leading Edge, v. 16, no. 4, p. 337–344. doi:10.1190/1.1437626

Dash, R.K., Sain, K., and Thakur, N.K., 2004. Overpressure detection from seismic amplitude versus offset response: an application to gas hydrates; Current Science, v. 86, no. 7, p. 985–990.

Dietrich, J.R., Coflin, K.C., Lane, L.S., Dixon, J., and Cook, F.A., 1989. Interpretation of deep seismic reflection data, Beaufort Sea, Arctic Canada; Geological Survey of Canada, Open File 2106, 15 p. doi:10.4095/130756

Dietrich, J., Chen, Z., Chi, G., Dixon, J., Hu, K., and McNeil, D., 2010. Petroleum plays in Upper Cenozoic strata in the Beaufort-Mackenzie Basin, Arctic Canada; *in* American Association of Petroleum Geologists, Annual Meeting Abstracts, American Association of Petroleum Geologists International Conference and Exhibition; Calgary, Alberta; September 12–15, 2010, 1 p.

Dix, C.H., 1955. Seismic velocities from surface measurements; Geophysics, v. 20, p. 68–86. doi:10.1190/1.1438126

Dixon, J. (ed.), 1996. Geological atlas of the Beaufort-Mackenzie area; Geological Survey of Canada, Miscellaneous Report 59, 173 p. doi:10.4095/207658

Dixon, J. and Dietrich, J.R., 1990. Canadian Beaufort Sea and adjacent land areas; *in* The Arctic Ocean Region: The Geology of North America, (ed.) A. Grantz, L. Johnson, and J.F. Sweeney; Geological Society of America, v. L, p. 239–256.

Dixon, J., Dietrich, J.R., and McNeil, D.H., 1992. Upper Cretaceous to Pleistocene sequence stratigraphy of the Beaufort-Mackenzie and Banks Island areas, Northwest Canada; Geological Survey of Canada, Bulletin 407, 100 p. doi:10.4095/133237

Dutta, N.V., 2002. Deepwater geohazard prediction using prestack inversion of large offset *P*-wave data and rock model; The Leading Edge, v. 21, no. 2, p. 193–198. doi:10.1190/1.1452612

Dvorkin, J., Mavko, G., and Nur, A., 1999. Overpressure detection from compressional- and shear-wave data; Geophysical Research Letters, v. 26, p. 3417–3420. doi:10.1029/1999GL008382

Foster, D.J. and Mosher, C.C., 1992. Suppression of multiple reflections using the radon transform; Geophysics, v. 57, p. 386–395. doi:10.1190/1.1443253

Hovland, M., Backman, J., Coakley, C., Collett, T., Darby, D., Foucher, J.P., Francis, T., Gelfgat, M., Gorshkovsky, A., Jokat, W., Kaminski, M., Kristoffersen, Y., Takahashi, K., Thiede, J., Wiley, C., and Zachos, J., 2011. The high-arctic drilling challenge: excerpts from the final report of the Arctic's role in Global Change Program Planning Group (APPG); JOIDES Journal, v. 27, p. 7–20.

Jin, Y.K. and Dallimore, S.R. (ed.), 2016. ARA05C Marine Research Expedition — Canada-Korea-USA Beaufort Sea Geoscience Research Program: Summary of 2014 Activities. Geological Survey of Canada, Open File 7999, 107 p. doi:10.4095/297866

Jin, Y.K., Riedel, M., Hong, J.K., Nam, S.I., Jung, J.Y., Ha, S.Y., Lee, J.Y., Conway, K.W., Kim, G.Y., Standen, G., Yoo, J., Kim, G., Ulmi, M., Neelands, P.J., and Dallimore, S.R., 2015. Overview of field operations during a 2013 research expedition to the southern Beaufort Sea on the RV *Araon*; Geological Survey of Canada, Open File 7754, 180 p. doi:10.4095/295856

Miley, M.P. and Kessinger, W.P., 1999. Overpressure prediction using converted mode reflections from base of salt; *in* 69th Annual International Meeting, Society of Exploration Geophysicists, Expanded Abstracts, Annual Meeting, 31 October to 5 November, 1999; Houston, Texas, p. 880–883.

Paull, C.K., Dallimore, S.R., Collett, T.S., Jin, Y.K., Mienert, J., Mangelsdorf, K., and Riedel, M., 2012. Drilling to investigate methane release and geologic processes associated with warming permafrost and gas hydrate deposits beneath the Beaufort Sea Shelf; IODP Pre-Proposal 806, <http://iodp.org/800> [accessed February 10, 2015]

Paull, C.K., Dallimore, S.R., Caress, D.W., Gwiazda, R., Melling, H., Riedel, M., Jin, Y.K., Hong, J.K., Graves, D., Sherman, A., Lundsten, E., Anderson, K., Lundsten, L., Villinger, H., Kopf, A., Johnson, S., Vrjenhoek, R., Conway, K., Neelands, P., and Côté, M., 2015. Active mud volcanoes on the continental slope of the Canadian Beaufort Sea; Geochemistry Geophysics Geosystems, v. 16, p. 3160–3181. doi:10.1002/2015GC005928

Pelletier, B.R., 1988. Marine science atlas of the Beaufort Sea: Geology and geophysics; Geological Survey of Canada, Miscellaneous Report 40, 39 p. doi:10.4095/126940

Pullan, S., MacAulay, M.H., Hunter, J.A.M., Good, R.I., Gagne, R.M., and Burns, R.A., 1987. Permafrost distribution determined from seismic refraction; *in* Marine Science Atlas of the Beaufort Sea: Geology and Geophysics, (ed.) B.R. Pelletier; Geological Survey of Canada, Miscellaneous Report 40, 37 p.

Riedel, M., Hong, J.K., Jin, Y.K., and Kim, H.S., 2014. Refraction seismic velocity analyses from multichannel seismic data acquired during Expedition ARA04C on the IBRV *Araon* in the Beaufort Sea; Geological Survey of Canada, Open File 7618, 67 p. doi:10.4095/295549

Riedel, M., Taylor, G., Taylor, A.E., and Dallimore, S.R., 2015a. Evidence for a deep gas hydrate stability zone associated with submerged permafrost on the Canadian Arctic Beaufort Shelf, Northwest Territories; Geological Survey of Canada, Current Research 2015-8, 17 p. doi:10.4095/296987

Riedel, M., Villinger, H., Asshoff, K., Kaul, N., and Dallimore, S.R., 2015b. Temperature measurements and thermal gradient estimates on the slope and shelf edge region of the Beaufort Sea; Geological Survey of Canada, Open File 7725, 143 p. doi:10.4095/296570

Shuey, R.T., 1985. A simplification of the Zoeppritz equations; Geophysics, v. 50, p. 609–614. doi:10.1190/1.1441936

Zoeppritz, R., 1919. On the reflection and propagation of seismic waves, Erdbebenwellen VIIIB; Göttinger Nachrichten, v. I, p. 66–84.

Geological Survey of Cananda Project 333209NP4X